



Communication Channels

Analysis of a LEO satellite communication link

Student: *Octavian GURLUI*

Professor: *Philippe DE DONCKER*

Teaching Assistant : *Nedid ISMAILI*

May 23, 2024

Contents

1	Introduction	3
2	Part 1 - Basic Scenario with Isotropic Antenna	4
2.1	Free Space Path Loss	4
2.2	Received Power	6
2.3	Signal-to-Noise Ratio	7
2.4	Channel Capacity	9
2.5	Total amount of transmitted data	10
2.6	Impact of Rain Attenuation	12
3	Part 2 - Antenna Array Effects	17
3.1	Antenna Radiation Patterns	17
3.2	Array Factors	18
3.3	Array Gain Patterns	21
3.4	Array Gains	24
3.5	Received Power	26
3.6	Signal-to-Noise Ratio	27
3.7	Channel Capacity and Total Transmitted Data	28
4	Part 3 - Setup involving two buildings	30
4.1	Evaluation of the LOS path	30
4.2	Evaluation of the reflected path	32
4.3	Evaluation of the diffracted paths	37

4.4	Re-evaluation of metrics	39
4.5	Limitations and Further Work	42
5	Conclusion	44

1 Introduction

Satellite communications have experienced a significant growth in interest and development, especially since large Low Earth Orbit (LEO) satellite constellations have started to be deployed. Unlike traditional geostationary satellites, which orbit at approximately 36,000 km above Earth, LEO satellites operate at much lower altitudes, typically between 500 and 2000 kilometers. The proximity to Earth enables LEO satellites to provide lower latency and higher data rates, therefore making them suitable for modern communication needs. Notable examples include SpaceX's Starlink and OneWeb, which aim to deliver high speed internet to even the most remote regions of the globe.

LEO satellites are highly suitable for applications that require global coverage and consistent connectivity. Operating in higher frequency bands such as Ku-band (10-12 GHz) and Ka-band (26-40 GHz) allows for greater bandwidth and data transmission capabilities - however these advantages come with challenges, such as signal attenuation due to atmospheric conditions, and the need for precise tracking systems.

The primary objective of this project is to analyze the downlink communication from a next-generation LEO satellite to a ground station, operating at 26 GHz. This analysis includes evaluating key performance metrics such as free path loss, received power, SNR, and channel capacity. Additionally, the project extends the evaluation by considering the use of antenna arrays at the ground station to enhance signal reception and directivity. Furthermore, the impact of a realistic geometric setup, involving two buildings adjacent to the ground station, is analyzed to understand the effects of multipath propagation, including LOS, reflected, and diffracted paths. By understanding these factors, it is possible to optimize satellite communication systems to meet the growing demand for high-speed, reliable internet connectivity across diverse environments.

2 Part 1 - Basic Scenario with Isotropic Antenna

In this part of the project, an analysis of the downlink communication from a LEO satellite to a ground station equipped with a single lossless isotropic antenna was performed. The overall objectives are to evaluate, during one satellite pass, certain metrics as a function of the satellite elevation:

- Free Space Path Loss
- Received Power
- Signal-to-Noise Ratio
- Channel Capacity
- Theoretical maximal transmitted data during one satellite pass

2.1 Free Space Path Loss

The free space path loss is a measure of the reduction in power of an electromagnetic wave as it propagates through free space. Channel loss due to free space propagation can be modelled using the Friis formula:

$$FSPL(dB) = -10\log_{10}G_{TX} - 10\log_{10}G_{RX} + 10n\log d + 20\log f - 147.5,$$

where:

- d is the distance between the transmitter and the receiver
- where λ is the wavelength of the signal, calculated as $\lambda = fc$, f being the frequency of the wave.

Therefore, the analysis of the communication link starts with a simple derivation of the distance between the transmitter and the receiver, based on the geometry of the setup. As it can be seen in fig. 1, this distance is shortest at the zenith position and increases as the satellite moves towards the horizon, which is expected. A python implementation for determining the distance d between the satellite and the receiver was performed based on the formula provided in the project specifications, which can be simply derived by considering the geometry problem seen in fig. 2.

The minimum distance is attained when the the satellite passes directly over the receiver, which corresponds to the satellite altitude of 500km, whereas the maximum distance occurs when the satellite is at horizon, and has been determined to be approx. 2573 km.

$$d = \sqrt{(R_e + h_s)^2 + R_E^2 \cos^2(E)} - R_E \sin(E)$$

Considering the situation where the satellite is at zenith, the general path loss model formula is used to determine the free space path loss for a distance of 500 km.

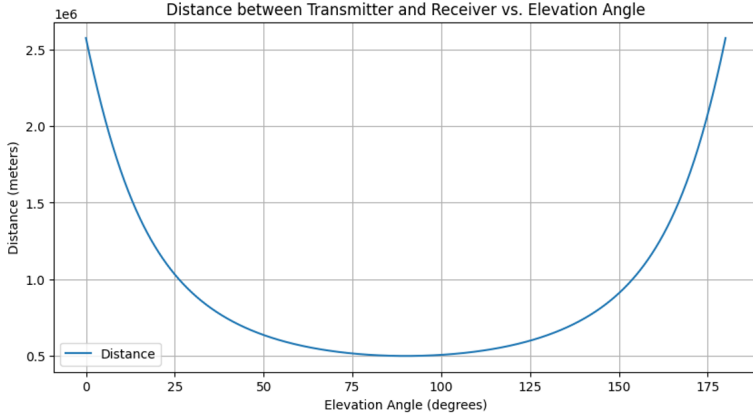


Figure 1: Distance between satellite and receiver based on the elevation angle

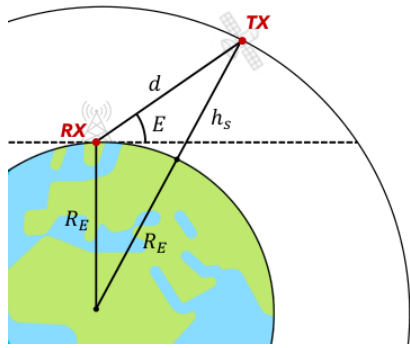


Figure 2: Determining the distance between satellite and receiver based on the elevation angle

Given the general path loss model,

$$L = 10\log_{10}\left(\frac{G_{TX}}{G_{RX}}\right) + 10n\log_{10}d + 20\log_{10}f - 147.5,$$

where $G_{TX} = G_{RX} = 1$ (assuming isotropic antennas), $n=2$ (assuming path loss coefficient for free space propagation), $d=500$ km, $f=26$ GHz,

$$\begin{aligned} L &= 10\log_{10}(1) + 10 \cdot 2\log_{10}(500 \cdot 10^3) + 20\log_{10}(26 \cdot 10^9) - 147.5 \\ &= 0 + 20\log_{10}(500 \cdot 10^3) + 20\log_{10}(26 \cdot 10^9) - 147.5 \\ &= 20\log_{10}(500 \cdot 10^3) + 20\log_{10}(26 \cdot 10^9) - 147.5 \end{aligned}$$

Breaking down the calculations,

$$20\log_{10}(500 \cdot 10^3) = 20(\log_{10}500 + \log_{10}10^3) = 20(2.699 + 3) = 20.5699 = 113.98dB$$

$$20\log_{10}(26 \cdot 10^9) = 20(\log_{10}26 + \log_{10}10^9) = 20(1.4149 + 9) = 20 \cdot 10.4149 = 208.298dB$$

Combining these terms, the free space path loss for $d=500$ km is determined to be

$$L = 113.98 + 208.298 - 147.5 = 174.778dB$$

Following similar calculations, the free space path loss for the situation when the satellite is at the horizon, therefore resulting in the highest path loss for the given geometry, has been determined.

$$L = 20\log_{10}(2573 \cdot 10^3) + 20\log_{10}(26 \cdot 10^9) - 147.5$$

$$L = 128.232 + 208.298 - 147.5 = 188.798dB$$

Therefore, assuming the free space path loss model, the loss experienced by the direct path between the satellite and the ground station varies between 175dB and 189dB, depending on the distance between the two. These results have been confirmed through a python implementation, as can be seen in fig.3.

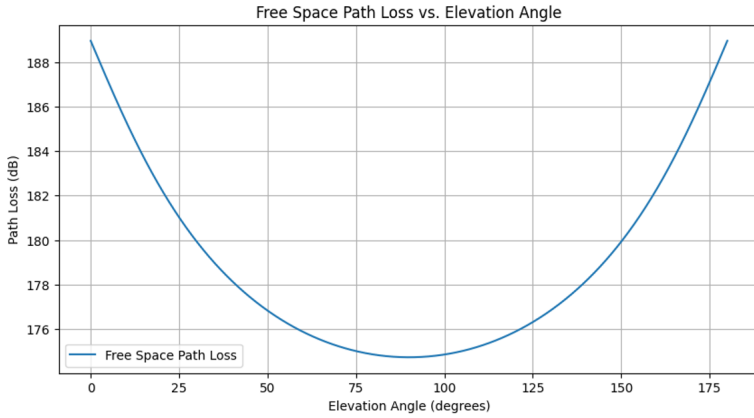


Figure 3: Free space path loss as a function of the elevation angle

The implementation confirms that the path loss is minimal when the satellite is directly overhead, when the distance between satellite and receiver is minimal, and increases the longer the signal has to travel.

2.2 Received Power

The received power at the ground station is calculated by subtracting the path loss from the Effective Isotropic Radiated Power (EIRP) of the satellite:

$$P_{RX} = EIRP(dBW) - PathLoss(dB) + 30,$$

where P_{RX} is the received power expressed in dBm, EIRP is the effective isotropic radiated power (expressed in dB) and the 30 accounts for unit conversion between W to mW.

The EIRP, the measure of power radiated by the satellite's antenna, has been provided in the project specifications with a specific value of 40 dBW.

Thus, a simple addition yields the received power as a function of the elevation angle, as it can be seen in fig.4. The received power is highest when the satellite is directly overhead and decreases as the elevation angle moves away from the zenith. The

values are negative because they are expressed in dBm, indicating the power received is less than 1 mW.

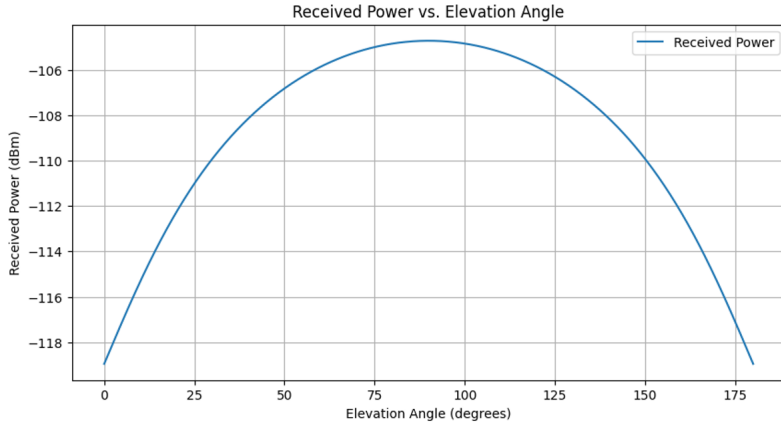


Figure 4: Received power as a function of the elevation angle

2.3 Signal-to-Noise Ratio

The Signal-to-Noise Ratio is calculated by comparing the received power to the total noise power. The total noise power has two contributions: thermal noise and receiver noise.

The thermal noise is calculated using $N = k_B \cdot TB$, where k_B is the Boltzmann constant, T is the temperature at the receiver end, and B is the bandwidth, as seen in [1]. The receiver noise is given by a noise figure F_{dB} , which has been specified in the project requirements. Therefore, the SNR (expressed in dB) is determined by:

$$SNR[dB] = P_{RX}[dBW] - F_{dB} - 10\log(k_B TB)$$

The project requirements specify the following parameters for the communication setup:

- Bandwidth: 40MHz
- Receiver noise figure: 2dB
- Receiver antenna temperature: 275K

A simple calculation based on the received powers obtained previously was performed. The lower values for the received power, obtained when the satellite is situated at horizon, have been determined to be around -118 dBm. Using the SNR formula seen above, it is possible to determine the SNR at 0 degrees of satellite elevation angle.

First, a conversion of the received power from dBm to dBW is needed:

$$P_{RX}[dBW] = P_{RX}[dBm] - 30$$

For -118 dBm,

$$P_{RX}[dBW] = -118 - 30 = -148dBW$$

To calculate the thermal noise power in dB,

$$N_{dB} = 10\log_{10}(K_B TB),$$

the values assumed in the project requirements have been used. The thermal noise power in Watts is:

$$N = k_B \cdot TB = 1.38 \cdot 10^{-23} \cdot 275 \cdot 40 \cdot 10^6 = 1.52 \cdot 10^{-13}W$$

Converted into dBW:

$$N_{dB} = 10\log_{10}(1.518 \cdot 10^{-13}) \approx -128.19dBW$$

Plugging in all the terms to determine the SNR,

$$SNR[dB] = -148 - 2 - (-128.19) = -21.81dB$$

If it is to consider the received power obtained when the satellite is at zenith, which is about -105dBm, the same calculation process renders:

$$P_{RX}[dBW] = -105 - 30 = -135dBW$$

$$SNR[dB] = -135 - 2 + 128.19 = -8.81$$

These calculations show a very poor signal quality, as the noise power exceeds the signal power by a significant margin, throughout the entire pass of the satellite over the ground station. The results have been confirmed and extended to the whole range of elevation angles through a python implementation, as can be seen in fig.5.

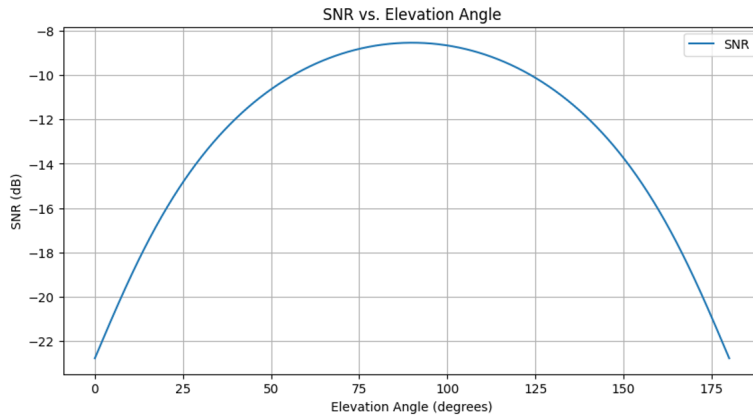


Figure 5: SNR as a function of the elevation angle

The SNR plot shows that the power of the signal is, at best, slightly over a tenth of the power of the noise, which is expected given the high path loss and the use of

an isotropic antenna. It is worth noting that in real-world scenarios, additional factors such as atmospheric conditions, multipath interference, and system noise would cause fluctuations in the SNR. However, this theoretical model assumes ideal conditions, resulting in a smooth SNR curve.

2.4 Channel Capacity

The channel capacity is calculated using the Shannon-Hartley theorem, which relates the bandwidth of the channel, the SNR, and the maximum achievable data rate. The formula for channel capacity C:

$$C = B \log_2(1 + SNR)$$

Using the previously determined values for the SNR corresponding to the situations where the satellite is either at horizon (SNR=-21.81dB) or at zenith (SNR=-8.81dB), a simple calculation shows the channel capacity for these specific scenarios. In the case of the maximum SNR value,

$$SNR(\text{linear}) = 10^{\frac{SNR(dB)}{10}}$$

$$SNR(\text{linear}) = 10^{\frac{-8.81}{10}} \approx 10^{-0.881} \approx 0.131$$

Given the bandwidth $B = 40 \cdot 10^6 \text{ Hz}$,

The channel capacity is

$$C = 40 \cdot 10^6 \log_2(1 + 0.131)$$

$$\log_2(1.131) = \frac{\log_{10}(1.131)}{\log_{10}(2)} \approx \frac{0.052}{0.301} \approx 0.173$$

$$C = 40 \cdot 10^6 \cdot 0.173 \approx 6.92 \cdot 10^6 \text{ bps}$$

Thus, with a SNR of -8.81dB and a bandwidth of 40MHz, the channel capacity is approximately 6.92Mbps.

Similar calculations have been performed for the satellite at horizon scenario. Due to the greater path loss, leading to worse SNR values, the channel capacity in this case has been determined to be lower:

$$SNR(\text{linear}) = 10^{\frac{-21.81}{10}} \approx 6.58 \cdot 10^{-3}$$

$$C = 40 \cdot 10^6 \log_2(1 + 6.58 \cdot 10^{-3}) = 40 \cdot 10^{-6} \log_2(1.00658)$$

$$C = 40 \cdot 10^{-6} \cdot 9.49 \cdot 10^{-3} \approx 379600 \text{ bps}$$

These results have been confirmed and extended through the whole range of elevation angles through a python implementation. Following a similar trend as the SNR, the channel capacity peaks at zenith and decreases towards the horizon, as seen in

fig.6. The area under the channel capacity curve represents the total transmitted data during the satellite's pass over the receiver.

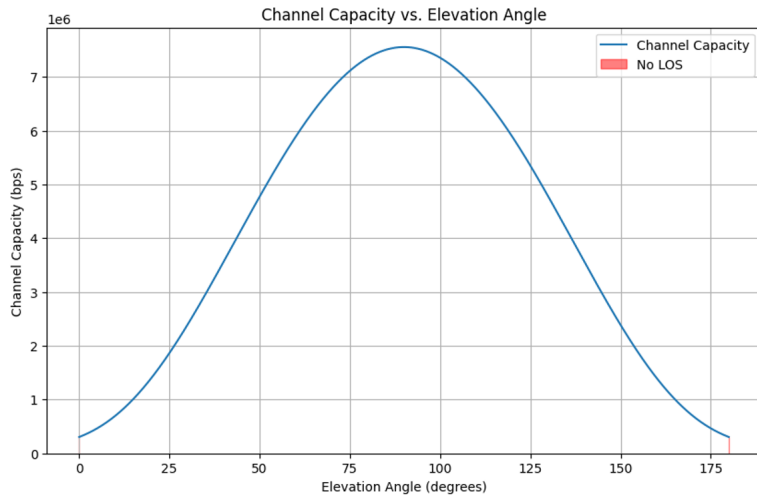


Figure 6: Channel capacity as a function of the elevation angle

2.5 Total amount of transmitted data

To calculate the total transmitted data, it is needed to integrate the channel capacity over the time the satellite is in line of sight (LOS) of the ground station. This requires considering the time the satellite spends at each elevation angle.

The LOS angle α represents the angular position of the satellite as seen from the ground station, considering Earth's curvature and satellite's altitude, as seen in fig.7. By knowing α , it is possible to accurately determine the time for the satellite to move between specific angular positions.

$$\alpha = \arcsin\left(\frac{d}{R_E + h_s} \cos(E)\right)$$

This step translates the satellite's position into angles that can be related to a part of the orbit trajectory, and therefore, to the revolution period. Essentially, the approach is to calculate the time for the satellite to traverse consecutive elevation angles, based on the revolution period. The segments where the elevation angle is between 0 and 180 degrees are summed to get the total LOS time.

The time interval for the satellite to move between the angle segments is given by

$$\Delta t_n = \frac{T_{rev} \cdot \Delta \alpha}{2\pi},$$

thus accounting for the fraction of the orbit corresponding to each angle segment.

The revolution period has been given in the project specifications as 5668s, therefore the time for which the satellite is within LOS from the ground station can be derived.

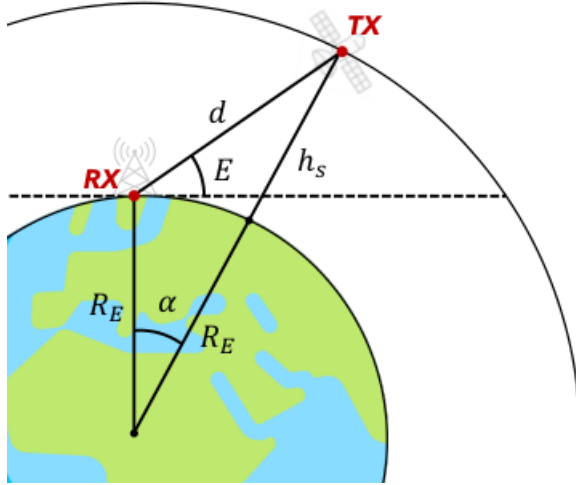


Figure 7: Geometry of the satellite trajectory and ground station

Using the law of cosines for the triangle formed by the Earth's centre, the satellite, and the receiver:

$$(R_E + h_s)^2 = R_E^2 + d^2 - 2 \cdot R_E \cdot d \cdot \cos(E)$$

$$\cos(\alpha) = \frac{R_E \cdot \cos(E)}{R_E + h_s}$$

The satellite is visible when it rises above the horizon until it sets below the horizon, corresponding to a range of E angles between 0 and 180 (therefore $\cos(E)=1$). This corresponds to alpha being 22.68 degrees when the elevation angle E=0:

$$\cos(\alpha) = \frac{R_E}{R_E + h_s} = \frac{6371 \cdot 10^3}{6871 \cdot 10^3} \approx 0.927$$

$$\alpha = \arccos(0.927) \approx 22.02\text{deg},$$

and conversely, alpha being -22.02 degrees when the satellite is at elevation angle E = 180 degrees. Therefore, this gives a range of alphas of 44.04 degrees.

This angle represents a fraction of $44.04/360 = 0.122$ of the orbit. In other words, for about 12% of the revolution period, the satellite is within the receiver's line of sight. Therefore, the LOS time can be derived:

$$\text{los time} = 0.122 \cdot T_{rev} = 0.122 \cdot 5668 = 692 \text{ seconds} \approx 11.54 \text{ minutes}$$

The total transmitted data is calculated by approximating the integral of the channel capacities over the LOS time. This is done using the trapezoidal rule:

$$\text{total transmitted data} = \sum \left(\frac{C_n + C_{n+1}}{2} \cdot \Delta t_n \right)$$

This approach takes into account the varying amounts of time the satellite spends at each elevation angle - as the satellite is approaching zenith, the time spent at the

elevation angle E intervals is shorter than at the intervals close to horizon, a fact that needs to be accounted for.

A simplified approach was also implemented, which considers that the satellite spends an equal amount of time at each elevation angle (11.54 minutes equally split between 180 degrees) - this is not entirely accurate but provides a quick sanity check. The channel capacity is calculated for a range of SNR values and an average capacity is determined; then, the total LOS time is then multiplied by this average capacity to estimate the total transmitted data.

The trapezoidal integration method renders a total transmitted data of approximately 174.1MB. By contrast, the simplified method which assumes equal time distribution, results in a higher estimate of 226.61MB.

Both methods indicate that the satellite can transmit a reasonable amount of data during its pass over the receiver, in spite of the relatively low SNR. Communication is therefore still possible, albeit with significant room for improvement - which can be performed by considering antenna arrays at the receiver end.

2.6 Impact of Rain Attenuation

Rain attenuation is a critical factor in satellite communication, especially at higher frequencies like 26 GHz. Rain can significantly affect the signal quality by increasing the path loss. The ITU recommendations provide methods to estimate the rain attenuation based on various parameters such as rain rate, elevation angle, slant-path distance, and specific attenuation [1].

The slant-path distance through rain is the distance that the signal travels through the rain, depending on the rain height and the elevation angle. The formula used is:

$$d_s = \frac{h_R}{\sin(E)},$$

where h_R is the rain height, and E the elevation angle.

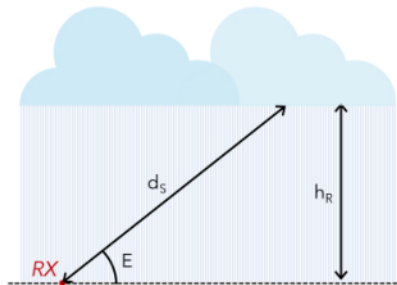


Figure 8: Slant-path length

The rain attenuation is determined using the specific attenuation γ and the slant-path distance:

$$L_r = \gamma \cdot d_s$$

The specific attenuation, expressed in dB/km, is given by an empirical model provided by the ITU:

$$\gamma = kR_{0.01}^\alpha,$$

where

- R is the rain rate (mm/h)
- k represents the baseline attenuation for a given frequency
- α characterizes the nonlinear effect of the rain rate on attenuation

The project requirements specify the rain height as 2.4km, and the coefficients have been derived from empirical data provided by the ITU. For Belgium and the Netherlands, the rain rate at 0.01% exceedance has been chosen as 30 mm/h, as per fig.9 [2]. This is interpreted as the percentage of a whole year when the rainfall exceeds 30 mm/h is less than 0.01%.

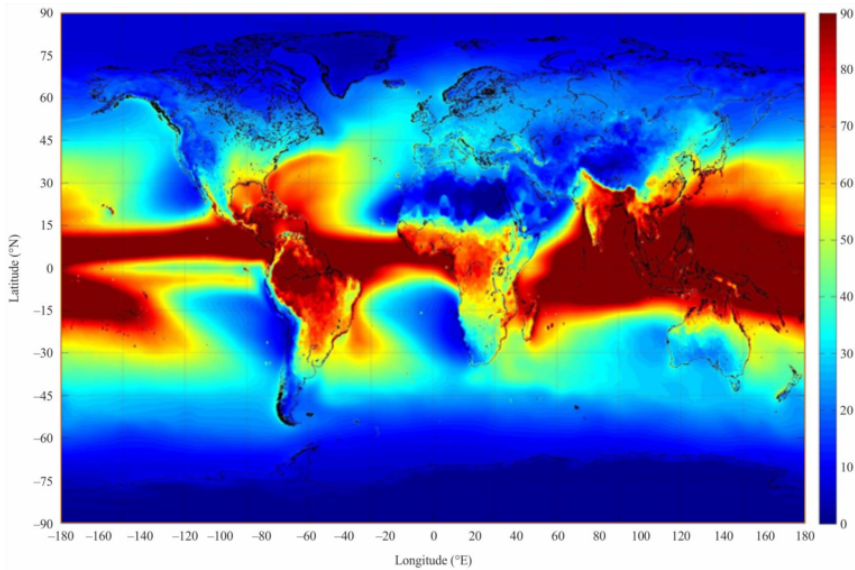


Figure 9: Rainfall exceeded for 0.01% of an average year. Illustration courtesy of ITU

The relationship between the exceedance percentage and rain attenuation is inverse. The higher the exceedance percentage (e.g., 1%), the lower the rainfall rate considered, resulting in lower rain attenuation values. Conversely, lower exceedance percentages (e.g., 0.01% or 0.001%) correspond to more extreme, less frequent rain rates, leading to higher rain attenuation values.

This relationship can be seen in fig.10, as the rain attenuation for different exceedances has been modelled for different elevation angles. More frequent but less intense rain events result in lower attenuation. Low exceedance percentages correspond to rare,

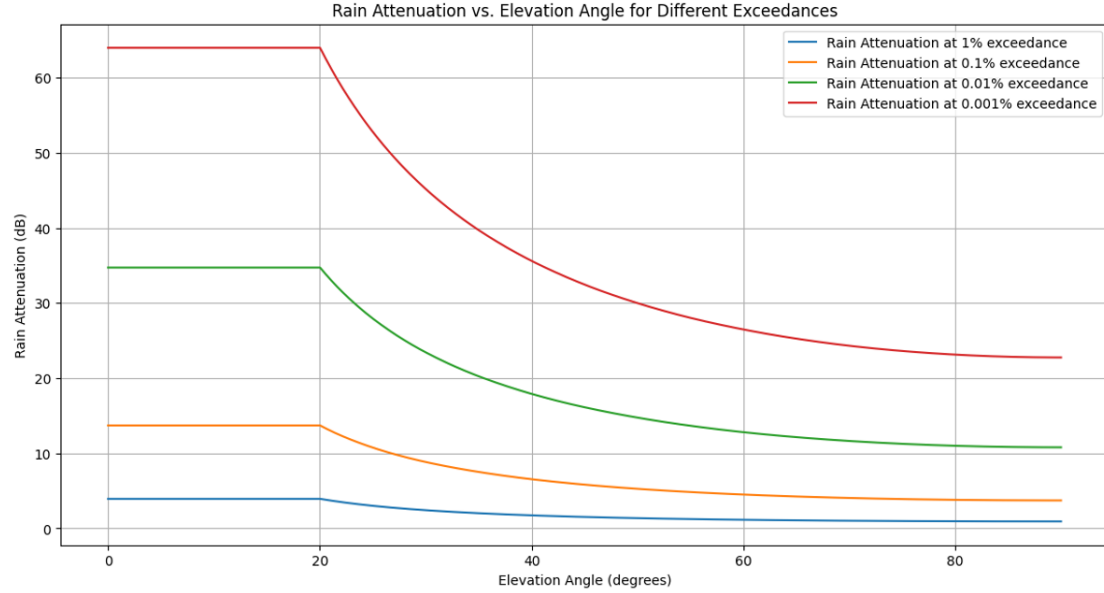


Figure 10: Rain attenuation for different exceedances

intense rain, resulting in higher attenuation.

Moreover, the plot in fig.10 also suggests the impact of the slant-path distance, which is expected, since the less distance the wave has to travel through rain, the less significant the impact of rain attenuation becomes. As per the project guidelines, for smaller elevation angles ($E \leq 20$ degrees), the rain attenuation has been considered constant and equal to the one computed at 20 degrees of elevation. This is likely because the simplified model used in this implementation is less accurate at low angles. This could be due to more variations in rain density, as the signal path through rain is longer, as well as other atmospheric effect like scattering being more significant. Therefore, to avoid inaccuracies, a constant attenuation value for angles below 20 degrees has been used.

The received power at the ground station is affected by rain attenuation. Thus, the adjusted received power considering rain attenuation for different exceedance percentages is calculated as follows:

$$P_{\text{rx, rain}}[\text{dBm}] = \text{EIRP}[\text{dBW}] + 30 - L[\text{dB}] - L_r[\text{dB}],$$

where L_r is the rain attenuation for different exceedance percentages.

The software model implementation confirms that received power decreases as the rain attenuation increases, as shown in 11. In the case of heavy rainfall, and especially at lower elevation angles, the received power is significantly lower than for the free space model. These findings are further reflected in the Signal-to-Noise ratio and the channel capacity, which have been evaluated in a similar manner to the free space scenario, but now using values adjusted for rain attenuation.

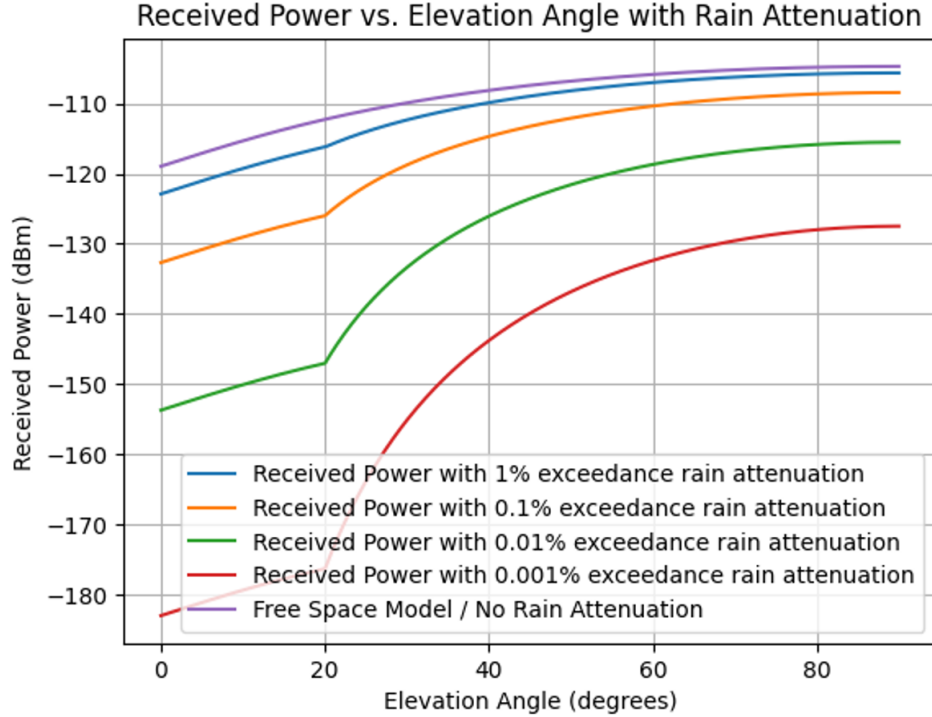


Figure 11: Received power at different rain exceedances

The SNR decreases as the rain attenuation increases, as seen in fig.12; high-intensity rain events (corresponding to lower exceedance percentages) significantly degrade the SNR. For high-intensity rain (0.001% exceedance), the SNR drops below -70 dB at lower elevation angles, making communication nearly impossible.

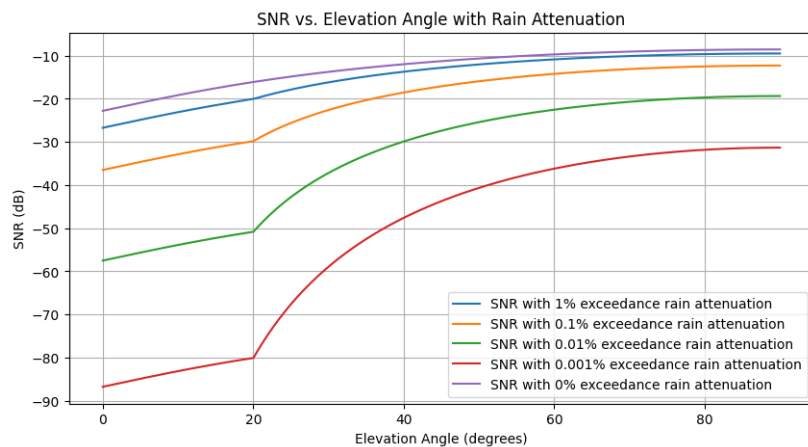


Figure 12: SNR at different rain exceedances

Furthermore, the channel capacity evaluated with the rain attenuation being considered, also highlights the significant impact of rainfall on the communication link (fig. 13). As for the total transmitted data during a satellite pass, using the same trapezoidal rule to approximate the integral of the channel capacity over time in LOS, the

following results have been obtained:

- Total transmitted data for 1% exceedance rain attenuation: 32.54 MB
- Total transmitted data for 0.1% exceedance rain attenuation: 14.83 MB
- Total transmitted data for 0.01% exceedance rain attenuation: 2.39 MB
- Total transmitted data for 0.001% exceedance rain attenuation: 0.13 MB

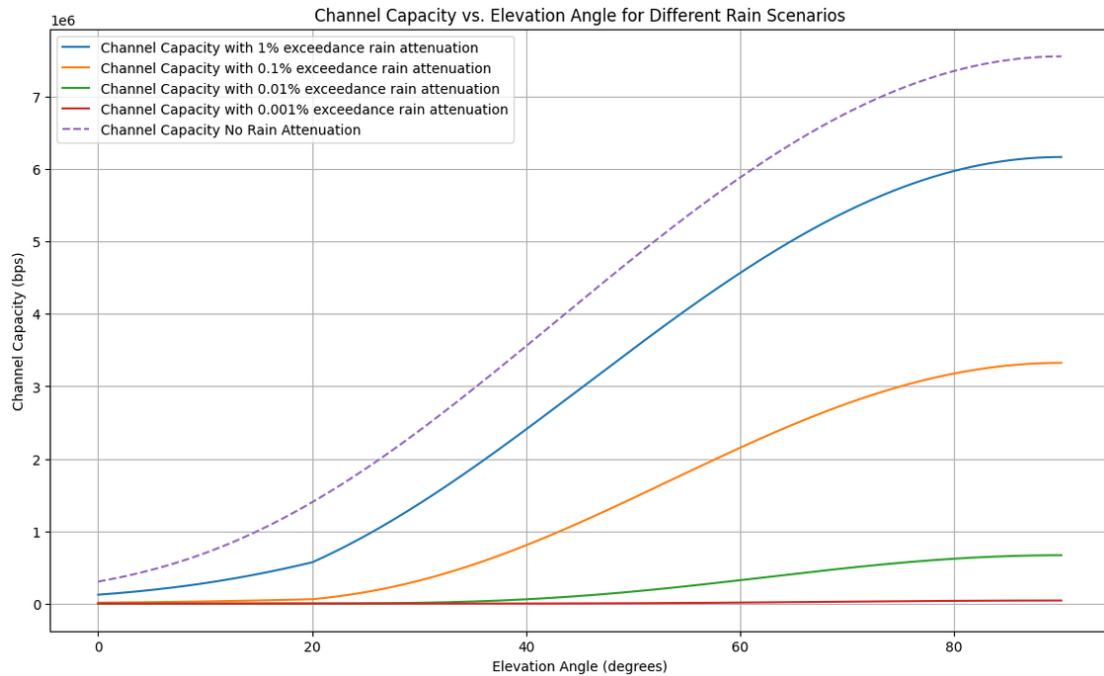


Figure 13: Channel capacity at different rain exceedances

It is therefore evident that heavy rain significantly reduces the channel capacity, especially at lower elevation angles, as the total transmitted data during one pass is considerably lower in heavy rain conditions compared to clear conditions.

These calculations provide a foundational understanding to the signal strength limitations due to distance and rain. In subsequent sections, additional factors will be incorporated, such as antenna array effects and multipath propagation for a more comprehensive analysis.

3 Part 2 - Antenna Array Effects

The first part of the project focused on the analysis of a downlink communication from a LEO satellite to a ground station equipped with a single isotropic antenna. While this provided a foundational understanding of the link characteristics such as free space path loss, received power, SNR and channel capacity, real-world scenarios often necessitate more sophisticated antenna configurations to improve signal reception.

In Part 2, the analysis is extended by considering the ground station equipped with a Uniform Linear Array (ULA) of antennas.

An antenna array consists of multiple individual antenna elements arranged in a specific geometric configuration. The primary advantage of using an antenna array is the ability to control the direction of the radiated signal through constructive and destructive interference of the signals from individual elements, through a process called beamforming. By adjusting the phase and amplitudes of the signals at each antenna array, it is possible to enhance the signal strength in specific desired direction, while minimizing interference from other directions.

The primary objective of this part is to evaluate the performance improvements offered by ULAs compared to a single isotropic antenna. The objectives thereby are:

- Compute the array gain for different ULA configurations
- Analyze the gain patterns of the ULAs
- Recalculate the key metrics from the first part - for the ULA configurations
- Interpret the implications of these findings on the overall link performance

3.1 Antenna Radiation Patterns

An isotropic antenna is an idealized model for an antenna which radiates power uniformly in all directions. It is a theoretical reference antenna with a gain of 1 (0 dB), therefore the radiation pattern is represented by a constant value in all directions.

By contrast, a patch antenna radiates more effectively in certain directions, creating a pattern with higher gain in the main lobe and lower gain elsewhere. The radiation pattern for a patch antenna is given by

$$U(\theta) = U_0 \sin^2(\theta),$$

where U_0 is a constant.

The individual antenna radiation patterns seen in fig.14 are used as building blocks for the subsequent steps in the implementation of antenna arrays.

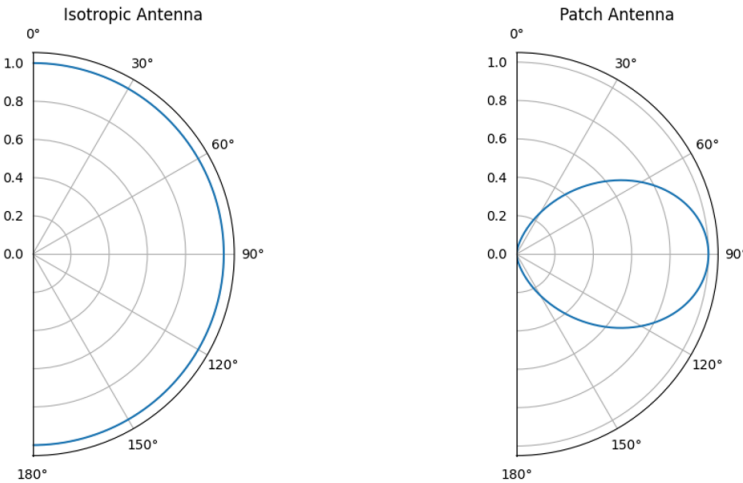


Figure 14: Isotropic and Patch antenna radiation patterns

3.2 Array Factors

The array factor is a mathematical representation of the combined radiation pattern of all elements in the array. It is a function of the number of elements, element spacing, and the direction of interest, the latter being determined by adjustments in the phase and amplitude of the signals from each element.

The general model for uniform linear arrays is:

$$AF(\theta, \phi) = e^{j(N-1)\phi/2} \frac{\sin(\frac{N\phi}{2})}{\sin(\frac{\phi}{2})},$$

where:

- $\phi = \beta d \cos(\gamma) - \delta$
- β is the phase constant given by $\beta = 2\pi/\lambda$
- d is the distance between antenna elements
- γ is the angle between the array axis and the direction of interest (where the array factor is evaluated)
- δ is the phase shift applied to each element

The angle γ is calculated as

$$\cos(\gamma) = \vec{I}_a \cdot \vec{I}_r,$$

where \vec{I}_a is the unit vector along the array axis, and \vec{I}_r is the unit vector in the direction of interest.

An evaluation of the array factor on a couple of basic cases of array configurations confirms that the python implementation that will be further used in this part of the project, is aligned with expectations.

For a first scenario, a linear array with 4 elements was considered, with a pointing angle of $\theta_m = 45$ degrees ($\pi/4$ radians), and the aim is to evaluate the array factor AF at 30 degrees ($\pi/6$ radians).

Using the wave frequency specified in the project requirements and the speed of light, the first step taken was determining the wavelength:

$$\lambda = \frac{26 \cdot 10^9 \text{Hz}}{3 \cdot 10^8 \text{m/s}} \approx 0.01154 \text{m}$$

The phase constant β is calculated as $2\pi/\lambda$, rendering approximately 544.64 radians per meter.

The element spacing d is considered as $\lambda/2 = 0.00577 \text{m}$

The phase difference ϕ was determined next:

$$\begin{aligned} \phi &= \beta d \cos(\gamma) - \delta \\ \phi &= 544.64 \cdot 0.00577 \cdot (\cos(\frac{\pi}{6}) - \cos(\frac{\pi}{4})) \\ \cos(\pi/6) &= \sqrt{3}/2 \\ \cos(\pi/4) &= 1/\sqrt{2} \\ \phi &= 544.64 \cdot 0.00577 \cdot (0.866 - 0.707) \\ \phi &\approx 3.14 \cdot (0.866 - 0.707) \\ \phi &\approx 0.499 \end{aligned}$$

And finally, evaluating the array factor AF:

$$\begin{aligned} AF(\theta, \phi) &= e^{j(N-1)\phi/2} \frac{\sin(\frac{N\phi}{2})}{\sin(\frac{\phi}{2})}, \\ AF &= e^{j(4-1)0.499/2} \frac{\sin(4 \cdot 0.499/2)}{\sin(0.499/2)} \\ AF &\approx e^{j(0.7485)} \frac{\sin(0.998)}{\sin(0.2495)} \\ AF &\approx e^{j(0.7485) \frac{0.841}{0.248}} \\ AF &\approx 3.39 \end{aligned}$$

This result aligns well with the python implementation of the array factor calculation for the same scenario, as it can be seen in fig.15.

A python code snippet has been used to evaluate the array factor for different configurations (4,8,16 elements) and pointing angles (0, 30, 45, 90 degrees).

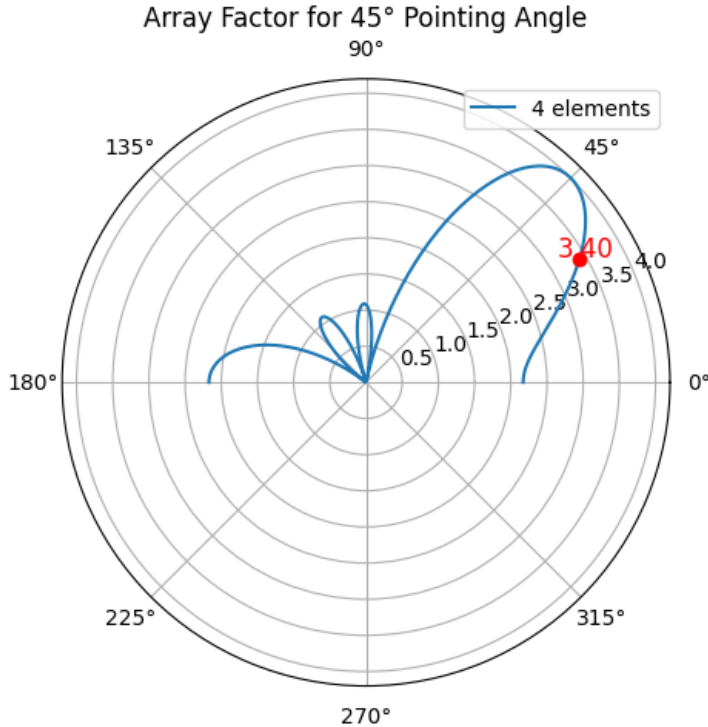


Figure 15: Array Factor for 4 elements, pointing angle 45 degrees

Figures 16, 17, 18 and 19 illustrate the array factors for ULAs with 4,8,16 angles, for pointing angles 0,30,45 and 90 degrees, respectively. These plots highlight several key characteristics of array behavior:

- In each figure, the main lobe is centered at the specific pointing angle. This demonstrates the beamforming capability of ULAs, where the array is able to steer its maximum radiation or reception in the desired direction by appropriately adjusting the phase of the signals at each element.
- The existence of side lobes in all figures, which is a common phenomenon in antenna arrays. Side lobes are the result of constructive interference occurring at angles other than the main lobe direction. While the main lobe represents the desired direction of maximum radiation, side lobes represent additional, less intense radiations at other angles.
- As the number of elements N increases, the beamwidth of the main lobe narrows, showing the increased ability to focus the beam more tightly in the desired direction. For instance, the main lobe in the 16-element array is much narrower compared to that in the 4-element array. However, an increase in the number of elements also results in more side lobes, because with more elements, there are more opportunities for constructive interference at various angles.

The array factors plots are normalized in order to help compare the relative strengths of the main and side lobes across different configurations.

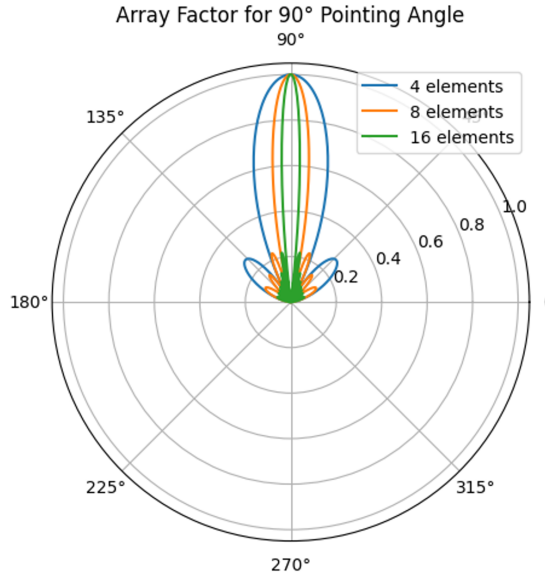


Figure 16: Array Factor for 4,8,16 elements, pointing angle 90 degrees (normalized)

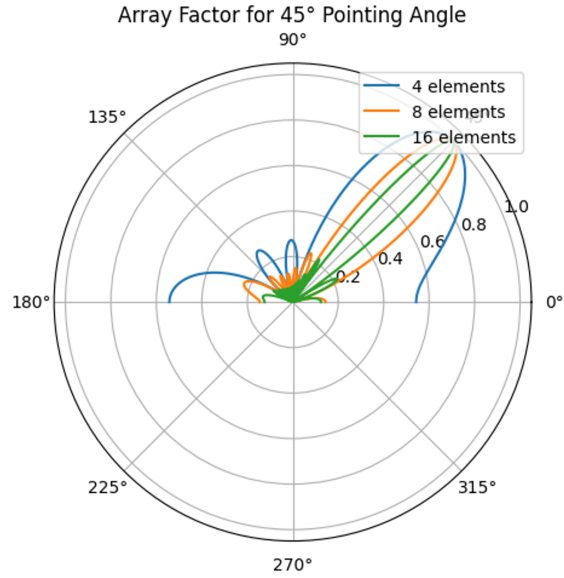


Figure 17: Array Factor for 4,8,16 elements, pointing angle 45 degrees (normalized)

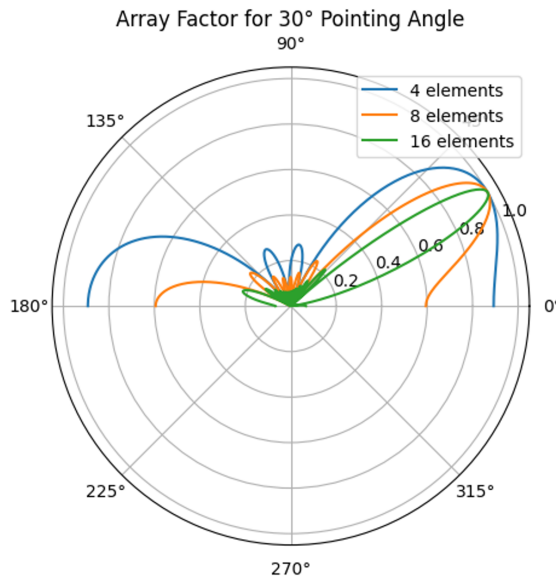


Figure 18: Array Factor for 4,8,16 elements, pointing angle 30 degrees (normalized)

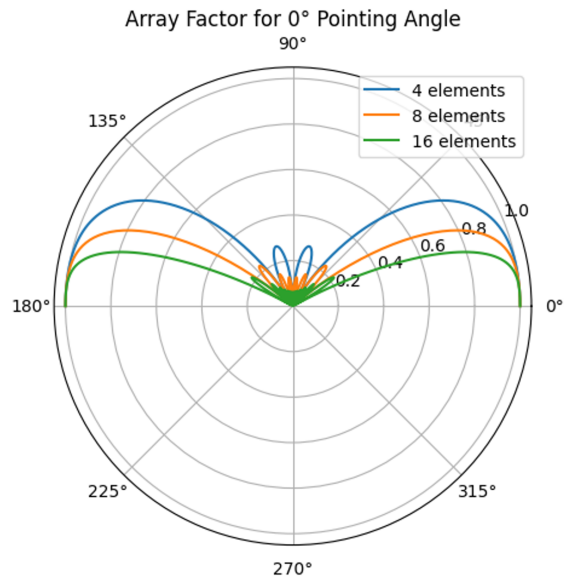


Figure 19: Array Factor for 4,8,16 elements, pointing angle 0 degrees (normalized)

3.3 Array Gain Patterns

To analyse the behavior of ULAs, both the individual radiation patterns of the array elements, as well as the collective effect of the array configurations, should be considered. The overall gain pattern of an array can be determined by combining the element pattern with the array factor:

$$U_{array}(\theta) = U_{SE}(\theta)|AF(\theta)|^2$$

Using the previously obtained results for the array factors given different config-

urations, and the individual radiation patterns of the isotropic and patch antennas, a straightforward implementation rendered the gain patterns for the different array configurations.

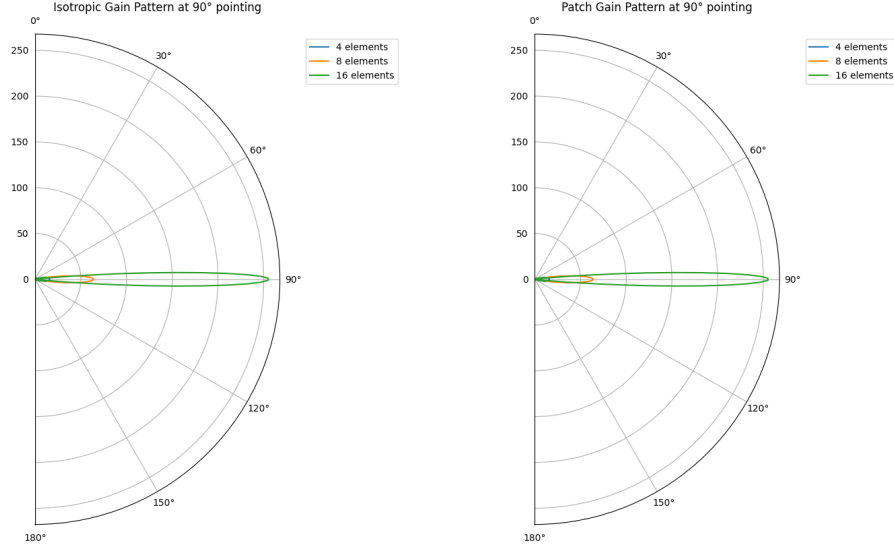


Figure 20: 4,8,16 element Isotropic and Patch array gain patterns, pointing angle 90 degrees

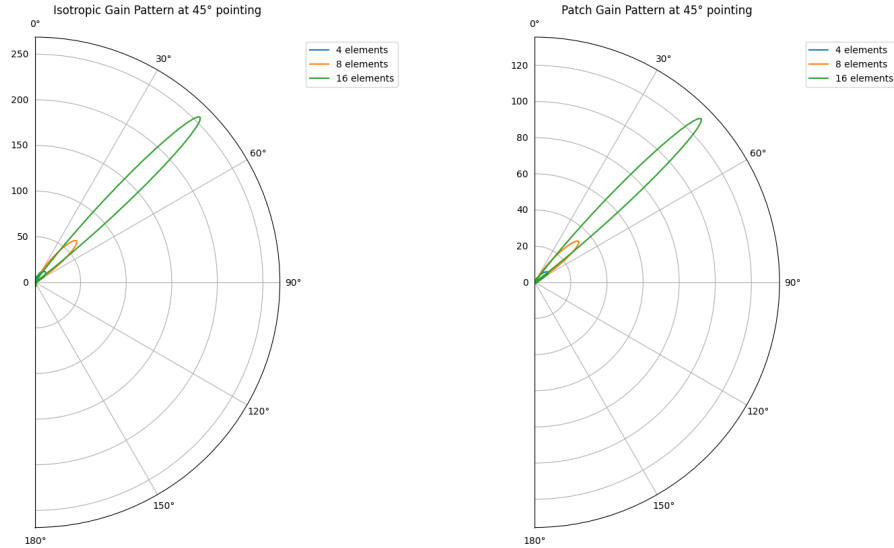


Figure 21: 4,8,16 element Isotropic and Patch array gain patterns, pointing angle 45 degrees

Figures 20, 21, 22 and 23 illustrate the array gain patterns for the 4,8,16-element ULAs using isotropic and patch antennas, at specific pointing angles. The gain patterns provide insights into the radiation characteristics and beamforming capabilities of the arrays, as follows:

- The magnitude of the main lobes increases with the square of the number of elements in the case of isotropic antennas. This is because the total radiated power is spread over a narrower beam as the number of elements increases, resulting

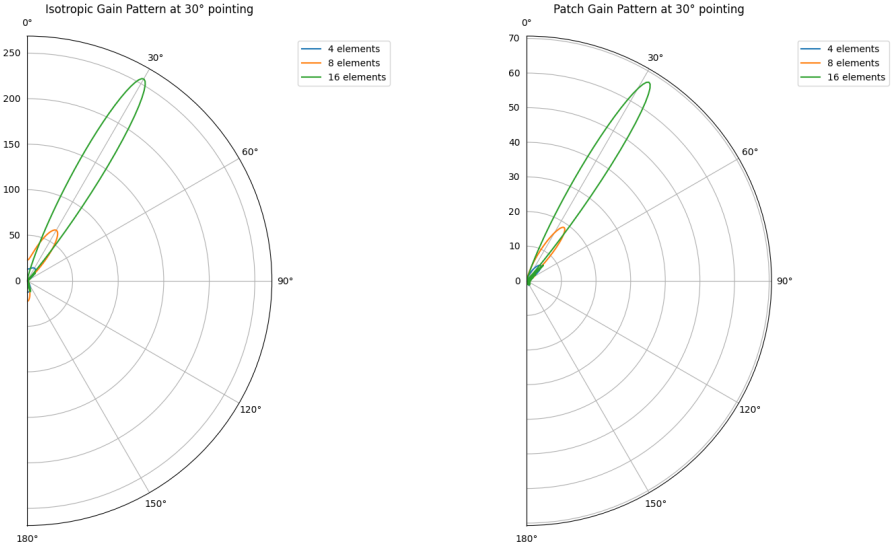


Figure 22: 4,8,16 element Isotropic and Patch array gain patterns, pointing angle 30 degrees

in a higher peak gain. The isotropic element pattern shows uniform gain across all directions, but as the number of elements increases, the array's beamforming capability becomes evident, focusing the energy in the desired direction.

- For patch antennas, the gain pattern is modulated by the element pattern $\sin^2(\theta)$, which causes the main lobe magnitude to vary with the pointing angle. At 90 degrees, where $\sin(90) = 1$, the main lobe magnitude coincides with that of isotropic arrays, while at other angles, the main lobe magnitude is reduced due to the squared sinus factor. While the peak gain might be lower than that of the isotropic antennas, patch antennas provide significant directivity, focusing the radiated power more effectively in the desired direction.
- As the number of elements increase, the main lobes become narrower for both isotropic and patch antenna arrays, a clear indication of increased directivity. Patch antennas exhibit even narrower main lobes compared to isotropic antennas, especially as the number of elements increases. This enhanced directivity is due to the combination of the directional element pattern and the constructive interference of the array elements.
- Both isotropic and patch antenna arrays show the presence of side lobes, which increase in number as the number of elements increases. Sidelobes are inherent to antenna arrays in general, but appear to be more numerous in the case of patch antenna arrays.
- Patch antenna arrays show poor beamsteering abilities at lower angles, as it can be seen in fig.19. Even though the pointing angle is set to 0 degrees, none of the lobes can be directed towards 0 degrees. Therefore, at lower angles, isotropic antenna arrays outperform the patch antenna arrays. This result is to be expected, due to the inherent limitation of the patch element pattern which has reduced gain at lower values.

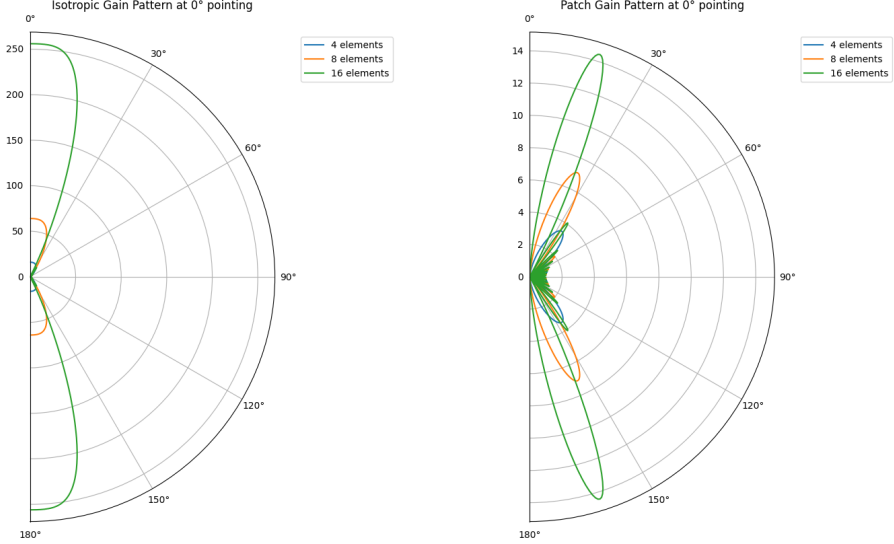


Figure 23: 4,8,16 element Isotropic and Patch array gain patterns, pointing angle 0 degrees

3.4 Array Gains

The gain pattern $U_{array}(\theta)$ shows the relative power distribution as a function of angle, but does not account for the total radiated power. The gain of an antenna array $G(\theta)$ is a normalized value that represents the effective gain in a given direction, considering the total power radiated by the antenna.

To find the total radiated power, the gain pattern $U_{array}(\theta)$ is integrated over all angles θ and ϕ . For a uniform linear array, this reduces to integrating over θ with a factor of 2π to account for ψ :

$$\int_{\Omega} U_{array}(\theta) d\Omega = 2\pi \int_0^{\pi} U_{array}(\theta) \sin(\theta) d\theta$$

And the actual gain of the array $G(\theta)$ is given by:

$$G(\theta) = \frac{U_{array}(\theta)}{\frac{1}{4\pi} \int_{\Omega} U_{array}(\theta) d\Omega}$$

For patch antenna arrays, despite the lower overall magnitudes of the main lobes, the narrower beamwidth results in higher normalized gain values. This is because the power is more concentrated in the direction of interest, leading to higher gain values in these directions, especially at higher elevation angles.

By contrast, isotropic arrays have wider main lobes compared to patch arrays. Because the power is spread out over a wider angle the normalized gain values are lower. However, at lower elevation angles, isotropic arrays can still exhibit higher gains due to their ability to steer beams more effectively in those directions.

These properties of patch and isotropic ULAs become apparent when plotting the gains of the different array configurations over all elevation angles, as seen in fig.24.,

with the assumption that the array is perfectly tracking the satellite, therefore the pointing angle is equivalent to the elevation angle at all times.

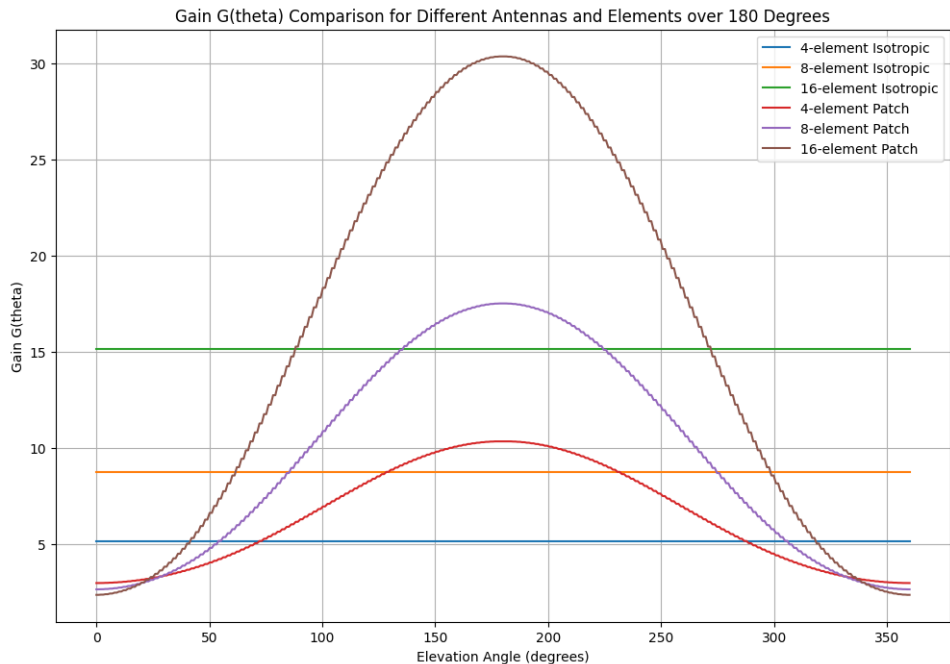


Figure 24: 4,8,16 element Isotropic and Patch array gains

The gain remains nearly constant across all angles in the case of 4,8 and 16-element isotropic arrays, which is to be expected. In addition, for an N -element isotropic array, the gain should be approximately N , to which the software implementation does align, albeit with some degree of inaccuracy, which most likely due to the integration method used. The gain was determined with the trapezoidal approximation method, rendering values of approximately 5 in the case of 4-element isotropic array, around 8 in the case of 8-element array, and slightly above 15 for the 16-element array.

In the case of 4,8 and 16-element patch arrays, the gain shows a pronounced peak at 90 degrees. The values obtained are around 10,15, and 25, respectively, which are reasonably aligned with theoretical expectations.

It is worth mentioning that the values obtained are unitless ratios. A gain of 8 is interpreted as the antenna array radiating 8 times more power in the specified direction than an isotropic antenna would. In the subsequent steps followed within the software implementation, like determining the received power, these values will have been converted to decibels.

The gain decreases more sharply away from the pointing angle due to the directional pattern of patch antennas. The results of this python implementation show that the gain of patch ULAs is higher as the antennas are pointed towards zenith, whereas the isotropic ULAs performs better at the lower elevation angles. This behavior turns

more in the favor of patch arrays when the number of array elements is increased - the patch ULA outperforms the isotropic ULA to an even higher degree as the number of array elements increase.

The observed gains and behavior are consistent with theoretical expectations and findings in the literature:

- For isotropic antennas, the gain is uniform in all direction, with each element equally contributing to the overall gain. The theoretical gain of an N -element isotropic array is approximately N .
- Patch antennas, being directional, have higher gain values when pointed at zenith, and the directional gain increases with the number of elements due to better focusing of the radiated energy.

3.5 Received Power

This section shows the investigation of the received power for the different antenna configurations previously considered. The objective is to evaluate how the array configurations affect the received power at different elevation angles, and to draw a comparison to the use of a single isotropic antenna at the receiver, as it has been considered in Part 1.

The gain $G(\theta)$, determined previously, is now being used to calculate the received power as follows:

$$P_{RX}[dBm] = EIRP[dBm] - \text{path loss}[dB] + G_{RX}(\theta)[dB]$$

Similar to the implementation of found in Part 1, the EIRP considered was 40dBW, given by the project specifications, and the path loss has been calculated based on the free space path loss model, varying with the distance between satellite and ground station.

As shown in fig.25, increasing the number of elements in the array improves the received power, which is to be expected due to the higher array gain when more elements are considered. Patch arrays exhibit a more pronounced peak at 90 degrees compared to isotropic arrays, reflecting the directional nature of patch antennas. The higher the number of elements, the sharper and higher the peak.

The results obtained highlight the practical implications of patch and isotropic ULAs. Patch arrays are ideal for applications requiring high gain in specific directions, which is the case for the satellite communication scenario at hand, where the angle of the satellite is known and can be tracked. The higher gain at the zenith improves the link quality.

Nevertheless, both isotropic and patch arrays offer significant improvements in received power compared to the usage of a single isotropic antenna at the receiver, as

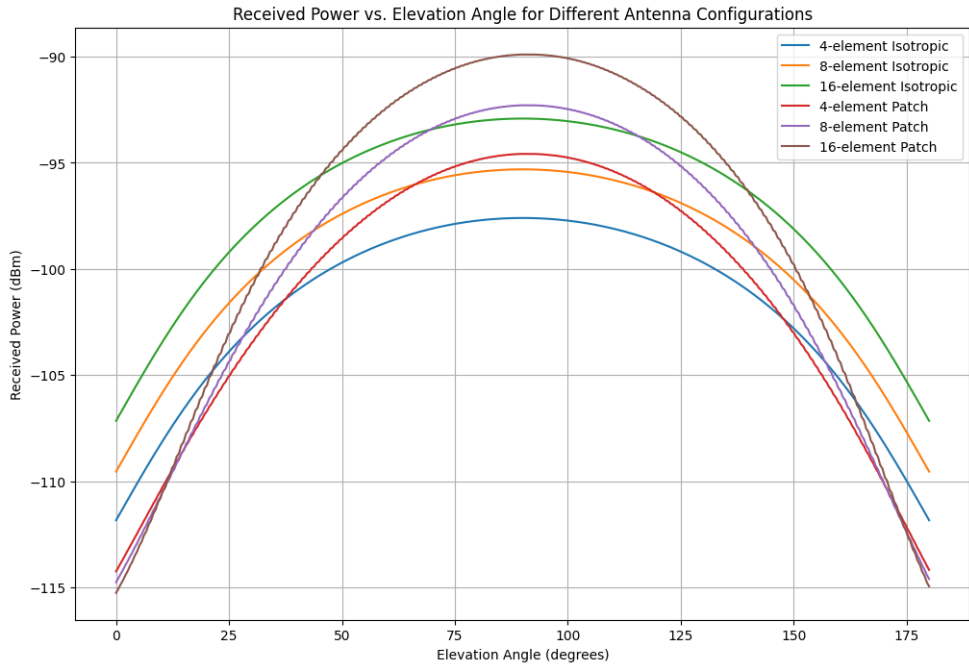


Figure 25: Received Power, considering 4,8,16 element Isotropic and Patch arrays

seen in Part 1. By comparison, the received power in that scenario were found to be at best -105dBm, at zenith, value which is outperformed by all array configurations. These improvements in received power directly translate to the other metrics to be evaluated, such as SNR, channel capacity and total transmitted data during one satellite pass.

3.6 Signal-to-Noise Ratio

The same steps followed for the SNR evaluation in Part 1 have been now used to determine this metric, considering the different array configurations.

The plot rendered by the python implementation (fig. 26) show a steady increase in the SNR for all array configurations, as the elevation angle increases, peaking at zenith, and decreasing below that. The highest SNR among the array configurations is achieved by the 16-element patch and isotropic arrays, respectively.

All of the antenna arrays configurations display significant improvements in SNR compared to the results obtained by using a single isotropic antenna at the ground station. Whereas the SNR in the case of using a single isotropic antenna ranges from -22 to -8dB, the array configurations (with the exception of the 4-element isotropic) were able to achieve positive SNR for a significant range of elevation angles.

Isotropic arrays provide a more uniform SNR across various elevation angles, therefore being practical for a broad area coverage, while patch arrays are preferable for applications requiring high SNRs in specific directions, such as the satellite communication link scenario at hand.

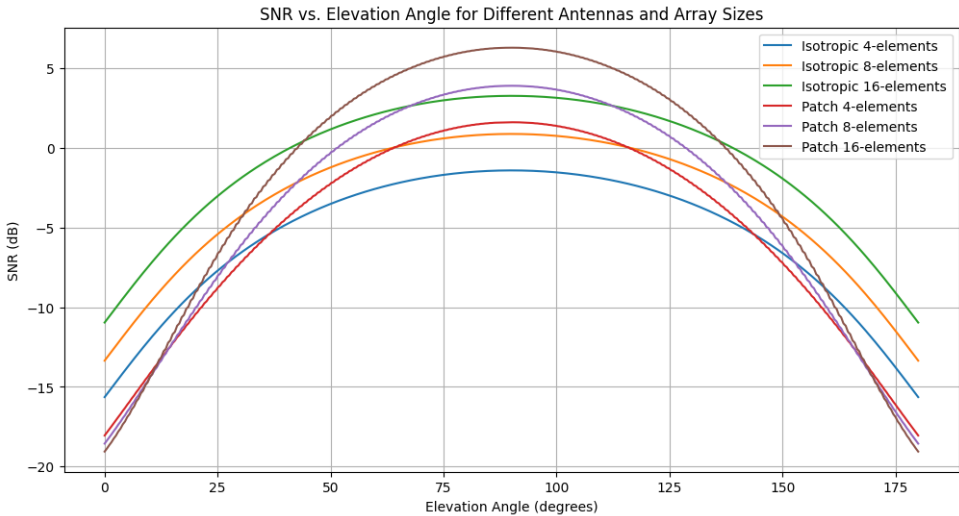


Figure 26: Signal-to-Noise ratio, considering 4,8,16 element Isotropic and Patch arrays

3.7 Channel Capacity and Total Transmitted Data

The channel capacity for each array configuration has been derived using the Shannon-Hartley theorem, as in Part 1. The newly evaluated metrics, shown in fig.27, display significant improvements over those obtained using a single isotropic antenna. The same trend observed in the previous metric follows, with the patch arrays outperforming the isotropic arrays for most elevation angles, exception being the range of angles close to horizon.

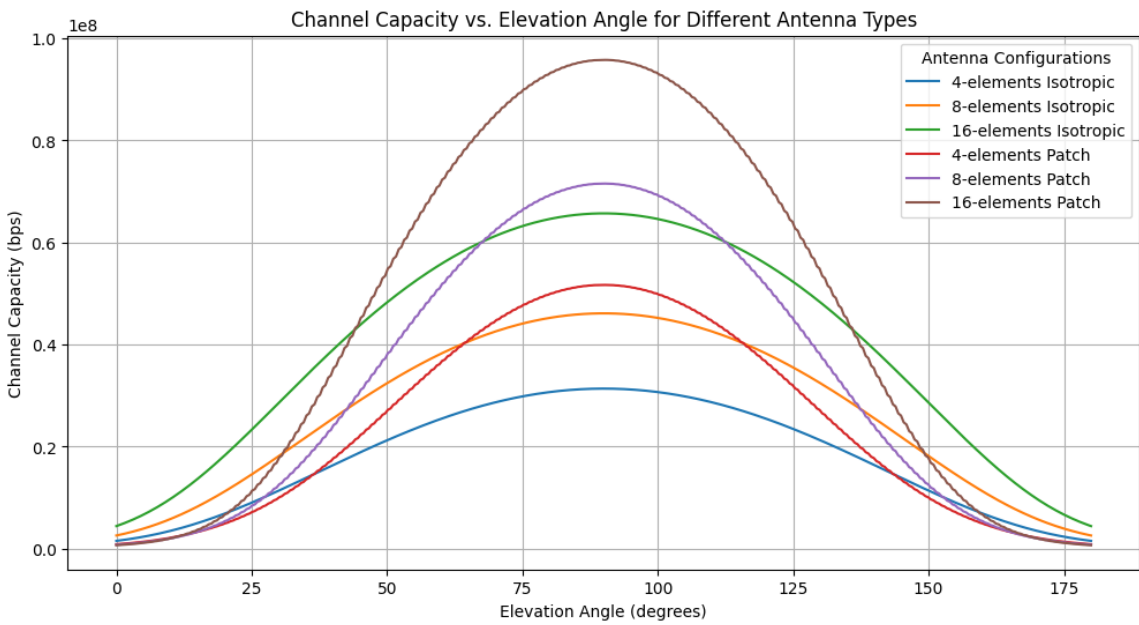


Figure 27: Channel capacity for different antenna array configurations

In terms of total data transmitted during one satellite pass, evaluated by computing the area under each channel capacity curve for every array configuration, have been

determined as such:

- isotropic 4-element array: 6040 MB
- isotropic 8-element array: 9153 MB
- isotropic 16-element array: 13553 MB
- patch 4-element array: 8224 MB
- patch 8-element array: 11306 MB
- patch 16-element array: 15536 MB

These results confirm the advantages of implementing ULAs at the receiver end, as the total amount of data that could theoretically be transmitted in one pass is orders of magnitude higher than in the case if a single isotropic antenna. Moreover, increasing the amount of array elements shows consistent improvements in terms of transmitted data, and this can be further enhanced by the usage of patch antenna arrays which provide better directivity.

4 Part 3 - Setup involving two buildings

In this section of the project, the analysis of the communication link between the satellite and the ground station has been expanded by incorporating additional environmental complexities: the presence of two buildings adjacent to the ground station. The objective is to analyse the impact of multiple propagation paths, including the direct line of sight (LOS), single reflections, and diffraction. This approach reflects a more realistic scenario where obstacles and multipath components significantly affect the signal strength.

The scenario involves the LEO satellite transmitting signals to a ground station equipped with different types of antennas. Two buildings, each 10 meters high, are positioned 10 meters apart on each side of the ground station, as it can be seen in fig.28. The satellite's orbit brings it directly overhead (at an elevation angle $E = 90$ degrees) before moving towards the horizon ($E = 0/180$ degrees of elevation).

The first step to be performed in this analysis is to identify the largest path for each elevation angle of the satellite, considering LOS, reflections, and diffraction.

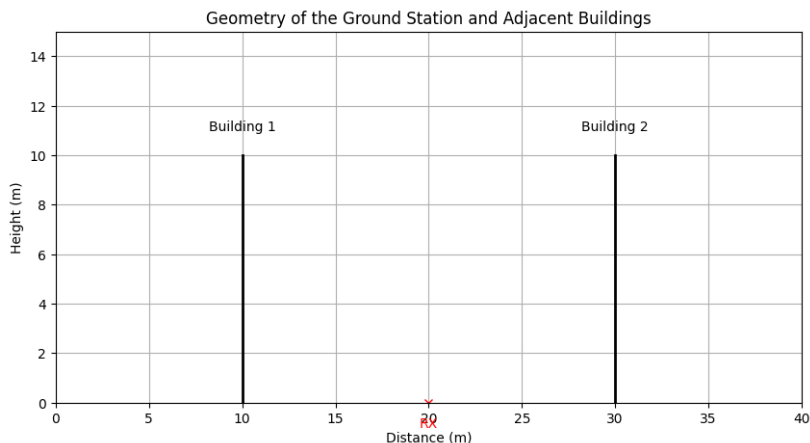


Figure 28: Geometry of the environment

4.1 Evaluation of the LOS path

The path loss of the LOS path can be directly inferred from the free space propagation path which has been modelled in Part 1, for the specific elevation angles where a straight, unobstructed path between the satellite and the ground station can be established.

In the software implementation, this scenario was evaluated in Cartesian coordinates, assuming the receiver positioned at the origin. The walls were located at (-0.01km, 0) and (0.01km, 0), with the tips of the walls at (-0.01km, 0.01km) and (0.01km, 0.01km), respectively. This setup allowed for the calculation of intersection points between the line connecting the satellite and the receiver and the walls. The satellite's

position, calculated based on the elevation angle in Cartesian coordinates, enabled the evaluation of the distance between the satellite and the ground station using Euclidean geometry. The results matched those obtained in Part 1, confirming the correctness of the implementation, as it can be seen in fig.29.

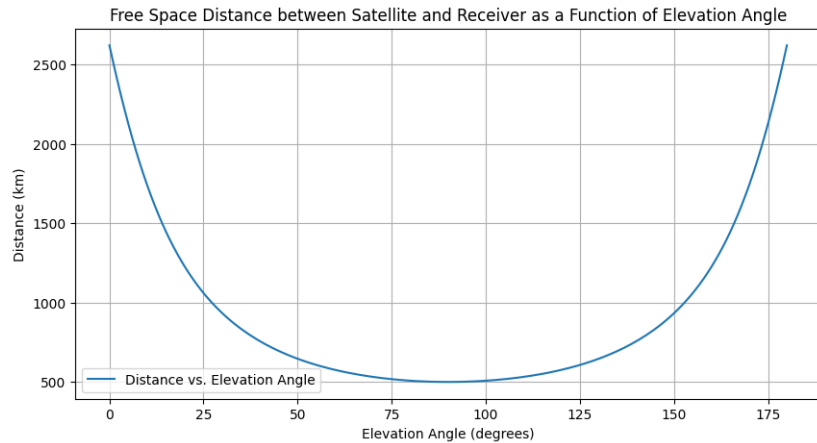


Figure 29: Free space distance between the satellite and ground station as a function of elevation angle

The free space path loss for the calculated distances was then evaluated using the same method as in Part 1.

The condition for the existence of LOS required that the direct line between the satellite and the receiver not intersect the wall on the same side as the satellite (the right wall for elevation angles below 90 degrees, and the left wall for angles above 90 degrees) at a height below the wall. To verify this, the line was evaluated at $x = 0.01$ (or $x = -0.01$). If the y -coordinate of the line at these points was less than the height of the wall, indicating obstruction, LOS was deemed not to exist for that elevation angle.

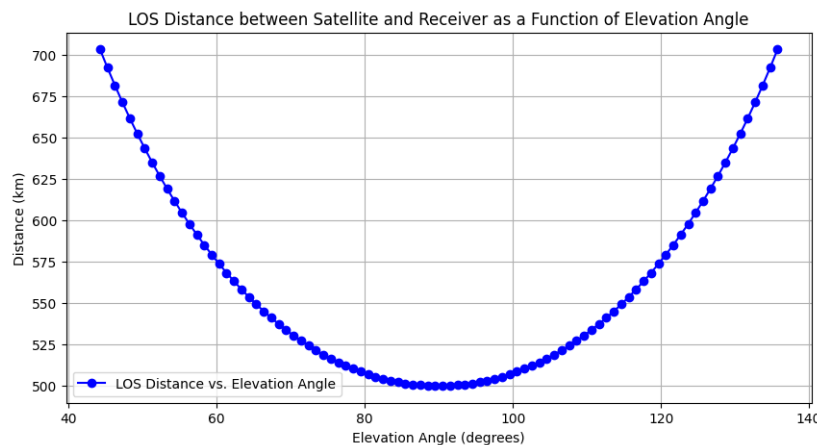


Figure 30: LOS Distance between satellite and receiver

As expected, given the 45-degree angles formed between the tips of the walls, their bases, and the receiver, the software implementation confirmed that LOS is possible for elevation angles within the range of 45 to 135 degrees, as illustrated in fig.30.

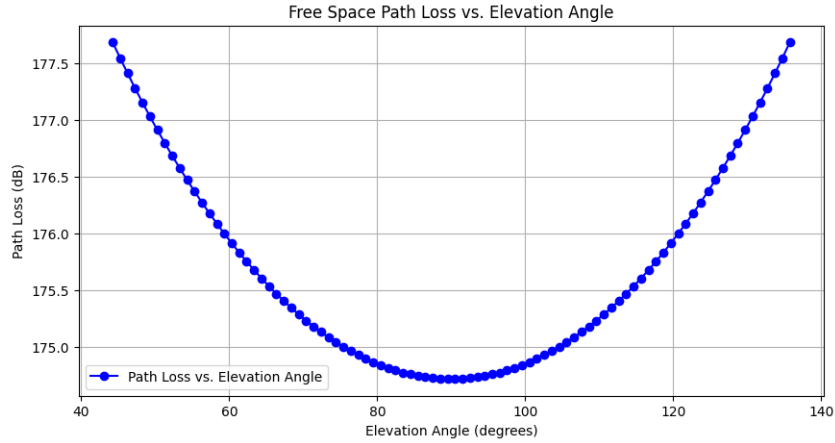


Figure 31: LOS pathloss between satellite and receiver

Therefore, for the elevation angles where LOS exists, the path loss values were retained. For the remaining angles, where LOS was obstructed, the values were discarded (fig.31).

4.2 Evaluation of the reflected path

To evaluate the reflected paths, the scenario where the satellite's signal reflects off one of the two buildings adjacent to the ground station was considered. The reflection conditions were assessed based on the satellite's position relative to the receiver and the buildings, using a geometric approach (mirror method). This method involves checking the feasibility of reflections based on the satellite's x-position and the walls' positions.

More specifically, if the satellite's x-position is positive ("right side of the receiver"), a potential reflection is considered with the left wall. A check is performed to assess whether the path between satellite's position (x_{sat}, y_{sat}) and the point $(-0.02, 0.00)$, evaluated at $x=-0.01$ (the left wall's position), intersects the wall between 0 and 0.01km (the wall's height). Conversely, if the satellite's x-position is negative ("left side of the receiver"), a reflection is considered with the right wall. If the path between the satellite's position and the point $(0.02, 0)$ intersects the wall at a y-coordinate below the wall's height, it is marked as a potential reflection.

In addition to the path intersecting the opposite wall, it also needs to clear the same-sided wall in order for a reflection to happen. That is, before the reflection with a wall even occurs, it requires that the path is not blocked by the other wall to begin with. More specifically, when the satellite is at $x > 0$, the path must also be above the right wall when evaluated at $x = 0.01$. Similarly, when the satellite is at $x < 0$, the path

must be above the left wall when evaluated at $x = -0.01$.

These conditions ensure that the reflected path is not obstructed by the wall on the same side as the satellite, allowing the evaluation of the elevation angles where reflection is possible. The results provided by the software implementation suggested that the reflections are possible within the elevation angle E ranges of 19-45 degrees, and 135-161 degrees.

For example, in the case of an elevation angle $E = 15$ degrees,

$$d = \sqrt{(R_e + h_s)^2 - (R_e \cos(\theta))^2} - R_e \sin(\theta),$$

where

$$R_e = 6371\text{km}, h_s = 500\text{km}$$

substituting the values,

$$d = \sqrt{(6371 + 500)^2 - (6371 \cos(15\text{deg}))^2} - 6371 \sin(15\text{deg}) \approx 1407.2\text{km}$$

the satellite position has been determined

$$x_{sat} = d \cos(\theta) = 1407.2 \cos(15\text{deg}) \approx 1359.25\text{km}$$

$$y_{sat} = d \sin(\theta) = 1407.2 \sin(15\text{deg}) \approx 364.21\text{km}$$

the slope of the reflected path is:

$$\text{slope} = \frac{y_{sat}}{x_{sat} - x_{\text{mirrored point}}}$$

$$\text{slope} = \frac{364.21}{1359.25 - (-0.02)} \approx 0.268$$

and the height where the path intersects the opposite wall is:

$$y_{\text{intersect opposite wall}} = \text{slope} \cdot (x_{\text{opposite wall}} - x_{sat}) + y_{sat}$$

substituting the values,

$$y_{\text{intersect opposite wall}} = 0.268 \cdot (-0.01 - 1359.25) + 364.21 \approx 2.68\text{m}$$

and the intersection height with the same-sided wall is:

$$y_{\text{intersect same side}} = \text{slope} \cdot (x_{\text{wall on same side}} - x_{sat}) + y_{sat}$$

substituting the values,

$$y_{\text{intersect same side}} = 0.268 \cdot (0.01 - 1359.25) + 364.21 \approx 8.04\text{m}$$

Therefore, when the satellite is at 15 degrees of elevation, there is no reflection, because the path towards a point of reflection is blocked by one of the walls.

At a 20 degree elevation angle,

$$d = \sqrt{(R_e + h_s)^2 - (R_e \cos(\theta))^2} - R_e \sin(\theta),$$

substituting the values,

$$d = \sqrt{(6371 + 500)^2 - (6371 \cos(20\text{deg}))^2} - 6371 \sin(20\text{deg}) \approx 1192.8\text{km}$$

the satellite position has been determined,

$$x_{sat} = d \cos(\theta) = 1192.8 \cos(20\text{deg}) \approx 1120.86\text{km}$$

$$y_{sat} = d \sin(\theta) = 1192.8 \sin(20\text{deg}) \approx 407.96\text{km}$$

following the same calculations for the slope of the reflected path, a slope of roughly 0.364 has been determined.

the intersection with the wall on the opposite side happens at:

$$y_{\text{intersect opposite wall}} = \text{slope} \cdot (x_{\text{opposite wall}} - x_{sat}) + y_{sat}$$

substituting the values,

$$y_{\text{intersect opposite wall}} = 0.364 \cdot (-0.01 - 1120.86) + 407.96 \approx 3.64\text{m}$$

and the intersection height with the wall on the same side as the satellite occurs at:

$$y_{\text{intersect same side}} = \text{slope} \cdot (x_{\text{wall same side}} - x_{sat}) + y_{sat}$$

$$y_{\text{intersect same side}} = 0.364 \cdot (0.01 - 1120.86) + 407.96 \approx 10.92\text{m}$$

Since the path clears the same sided wall and falls below the height of the opposite wall, a reflection does occur in the case of a satellite elevation angle of 20 degrees.

Considering the range of angles for which reflection is possible, the reflected path distance has been computed and plotted, as seen in fig.32. Since the additional distance added due to reflection is minimal compared to the distance between the satellite and the ground station, the values obtained are similar to those obtained in the case of LOS paths.

To determine the path loss for the reflected paths, it is needed to account for the reflection introducing the reflection coefficient Γ , evaluated based on incidence angle and the electric permittivity ϵ_r of the reflected surface.

$$\Gamma = \left| \frac{\epsilon_r \cdot \cos(\theta) - \sqrt{\epsilon_r - \sin^2(\theta)}}{\epsilon_r \cdot \cos(\theta) + \sqrt{\epsilon_r - \sin^2(\theta)}} \right|,$$

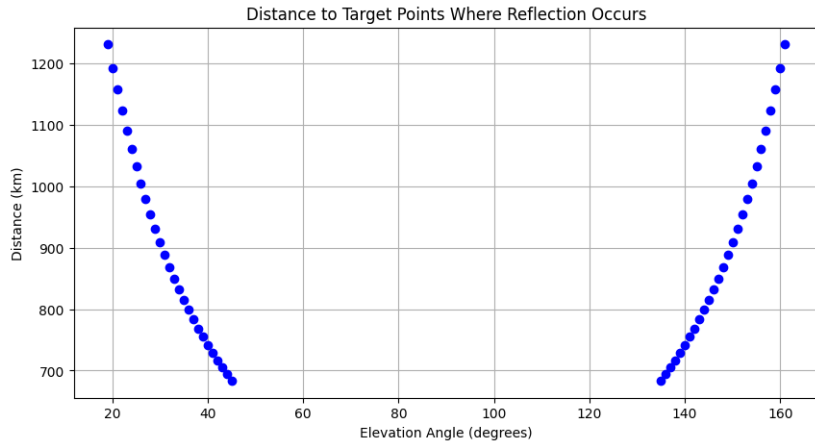


Figure 32: Reflected Path Distance between satellite and receiver

where the relative permittivity of the building walls has been specified in the project requirements.

The reflected path loss $L_{\text{reflected}}$ is therefore determined using:

$$L_{\text{reflected}} = L_{\text{LOS}} + 20 \log_{10}(\Gamma)$$

The resulting plot (fig.33) shows the reflected path loss for angles where reflections occur.

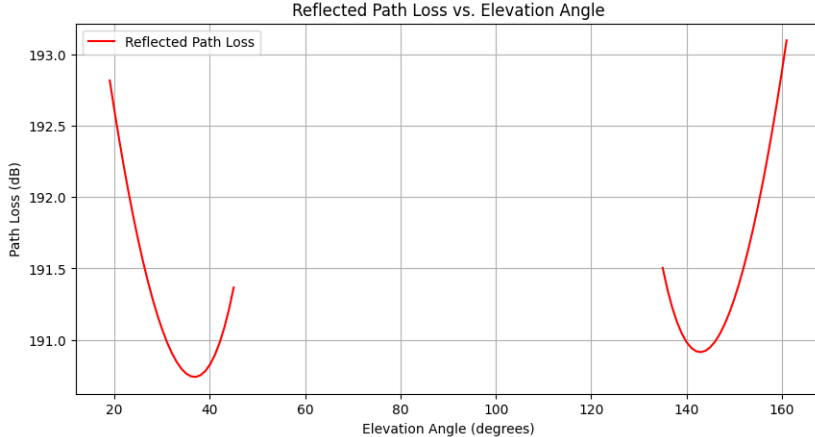


Figure 33: Reflected Path Losses

It is therefore easy to see that reflections introduce additional path loss compared to direct LOS paths, as the reflected path losses are higher than LOS path losses.

The path loss shows minima at certain elevation angles, suggesting that there are preferred angles where the reflection loss is minimized. This is could be due to the influence of the reflection coefficient - the angle at which the waves hit a reflective surface can significantly affect the strength of the reflected signal. If the incident angle

aligns such that the wave strikes the surface more directly (perpendicular), the reflection might be stronger compared to more acute angles, therefore this can reduce the path loss compared to other angles.

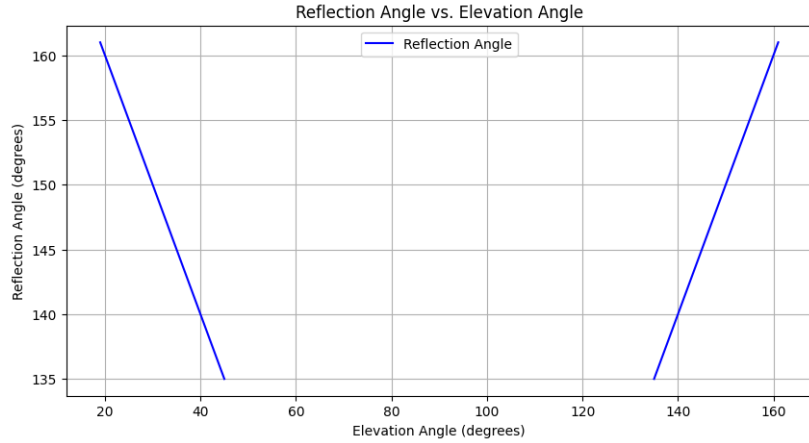


Figure 34: Angle of Reflection plotted over the satellite's elevation angle

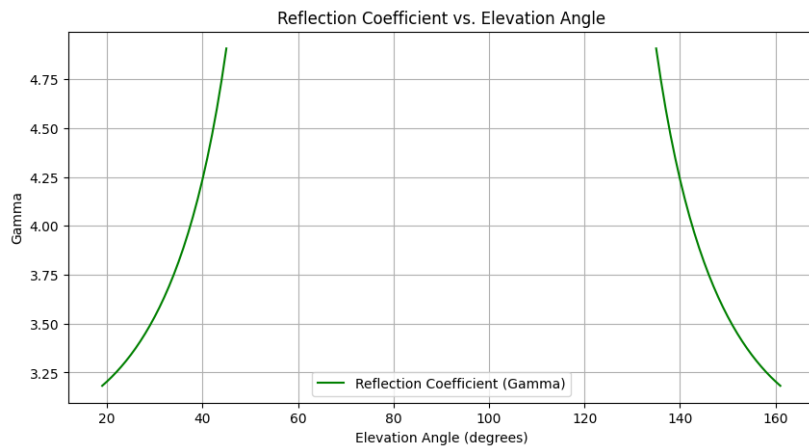


Figure 35: Reflection Coefficient

Indeed, the reflection angle becomes closer to 90 degrees as the satellite moves towards zenith, as seen in fig.34, and this leads to an increase in the reflection coefficient (fig.35.). This can be interpreted as more power being reflected at higher angles. Paired with the shorter travelled path distance, this should result in a lower reflected path loss as the elevation angle is increased, which does not explain the dips observed in fig.33.

While the overall trend shows a decrease in reflected path loss as the satellite moves towards zenith, the exact nature of the dips and the overall pattern requires further investigation. Due to time constraints, a deeper investigation into these factors was not possible, but the observed trends still provide valuable insights into the behavior of reflected paths in satellite communication.

4.3 Evaluation of the diffracted paths

In this section, the impact of diffracted paths on the received signal strength was evaluated. Diffraction occurs when the signal encounters obstacles such as buildings, causing the wave to bend around the edges of the obstacle. The knife-edge diffraction model was used to estimate the diffraction loss for the given scenario.

Diffraction loss can be calculated using the knife-edge model, which simplifies the problem by assuming a single sharp edge (or knife-edge). The loss depends on the relative height of the obstacle and the distance between the transmitter, obstacle, and receiver. The key Fresnel parameter ν , used to calculate the diffraction loss, is given by:

$$\nu = h \sqrt{\frac{2}{\lambda} \left(\frac{1}{d_1} + \frac{1}{d_2} \right)},$$

where:

- h is the effective height of the obstacle above the line of sight
- λ is the wavelength of the signal
- d_1 is the distance from the transmitter to the obstacle
- d_2 is the distance from the obstacle to the receiver

The diffraction loss L_{ke} can be then calculated as:

$$L_{ke} = 10 \log_{10}(|F(\nu)|^2),$$

where $F(\nu)$ is the Fresnel integral.

To evaluate the diffraction loss, the following steps were undertaken:

1. Calculation of the satellite position: determined for each elevation angle using Cartesian coordinates, as it has been done in the previous steps
2. Determination of Effective Height h : done by finding the vertical distance from the satellite to the tip of the wall: $h = y_{sat} - \text{wall height}$, where y is the perceived height of the satellite above the observer's horizon (not to be confused with the satellite's altitude)
3. The horizontal distance from the satellite to the wall where diffraction is considered, d_1 , is $d_1 = |x - \text{wall } x|$, while the horizontal distance from the wall to the receiver d_2 is fixed at 10 meters.
4. Finally, the parameter ν for knife-edge diffraction model is calculated given the formula above. To obtain the diffraction path loss L_{ke} , it is needed to evaluate the Fresnel integral $F(\nu)$ first. The following approximation is considered:

$$|F(\nu)|^2 \approx \frac{1}{2\pi^2\nu^2}$$

Evaluation the parameter ν for the scenario where the satellite is at horizon,

$$h = 0.01, d_1 \approx 2500\text{km}, d_2 = 0.01\text{km}$$

$$\begin{aligned}\lambda &= \frac{c}{f} = \frac{3 \cdot 10^8}{26 \cdot 10^9} \text{m} = 0.01154\text{km} \\ \nu &= h \sqrt{\frac{2}{\lambda} \left(\frac{1}{d_1} + \frac{1}{d_2} \right)}\end{aligned}$$

plugging the values in,

$$\begin{aligned}\nu &= -0.01 \sqrt{173.31 \left(\frac{1}{2500} + 100 \right)} \\ \nu &= -0.01 \sqrt{173.31 (0.004 + 100)} \\ \nu &= -0.01 \sqrt{17331.69} \\ \nu &= 0.01 \cdot 131.65 \\ \nu &\approx 1.316\end{aligned}$$

And in the case the satellite is at 80 degrees of elevation,

$$\begin{aligned}h &= 499\text{km}, d_1 = 88.05\text{km}, d_2 = 0.01\text{km} \\ \nu &= 499 \sqrt{\frac{2}{0.01154} \left(\frac{1}{88.05} + \frac{1}{0.01} \right)} \\ \nu &= 499 \sqrt{173.31 \left(\frac{1}{88.05} + 100 \right)} \\ \nu &= 499 \sqrt{173.31 (0.01136 + 100)} \\ \nu &= 499 \sqrt{17333.68} \\ \nu &= 499 \cdot 131.67 \\ \nu &\approx 65602.33\end{aligned}$$

The manual calculations align with the trends observed in the plot seen in fig.36, provided by the software implementation.

The computed values do not align with the expected physical behavior. Intuitively, it would be expected for the diffraction loss to be minimal when the ray between the satellite and the receiver is bent the least, such as at elevation angles close to 45 degrees. At these angles, the impact of diffraction should be minimal, and the diffraction loss should be low. Conversely, at other angles where the bending is more significant, the impact of diffraction should increase, resulting in higher diffraction losses.

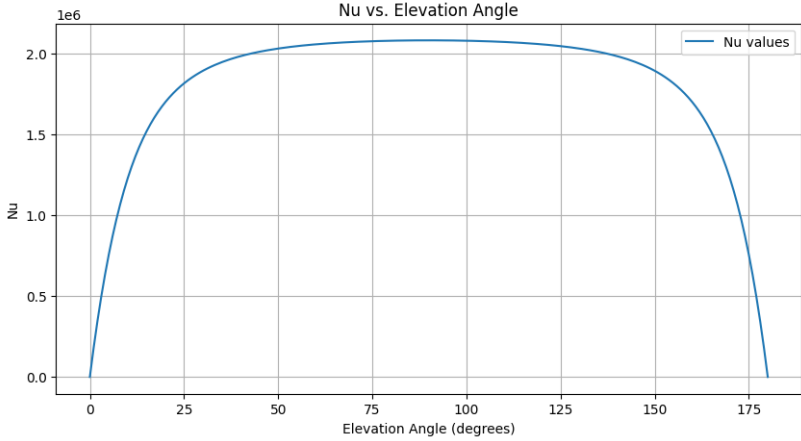


Figure 36: Fresnel Parameter

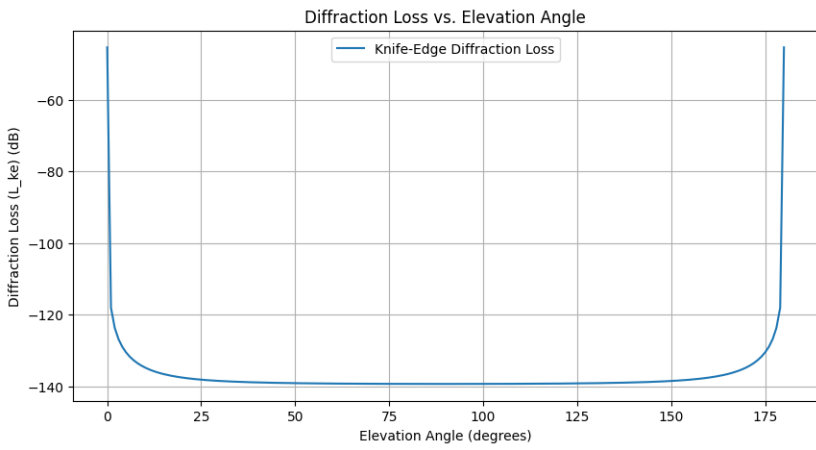


Figure 37: Diffraction Loss

However, this expected behavior is not reflected in the current evaluation of the Fresnel parameter ν or the diffraction loss versus elevation angle plot (37). The diffraction loss values are negative, which is not physically interpretable, as loss values should be positive. Therefore, it suggests that there might be an error in the current implementation or evaluation of the diffracted path loss. However, due to time constraints, it was not possible to identify the exact source of these erroneous values.

4.4 Re-evaluation of metrics

In this subsection, a reevaluation of the metrics from Part 1 of the project has been performed, incorporating the effects of the strongest multipath component. This analysis considers the component with the lowest path loss, which could be either the direct LOS path, a reflected path, or a diffracted path, depending on the elevation angle.

The path loss is evaluated over the range of elevation angles from 0 to 180 degrees. The minimal path loss at each elevation angle is determined by considering the following:

- If a direct LOS path exists, it typically represents the minimal path loss due to the unobstructed propagation of the signal.
- In cases where LOS does not exist, the strongest reflected path (if any) is considered. The reflection loss is influenced by the reflection coefficient, which varies with the reflection angle.
- For elevation angles where neither LOS nor reflections occur, the diffracted path loss is considered, since the path losses for diffracted paths have been determined to be the highest across all elevation angles.

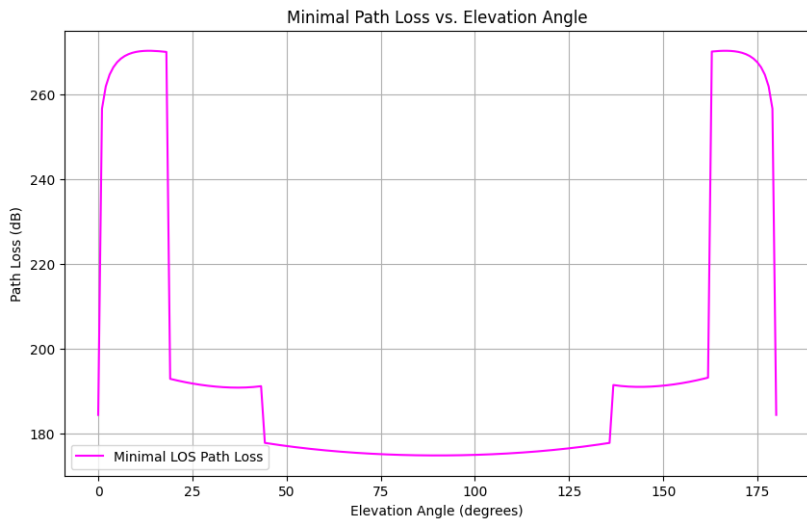


Figure 38: Minimal Path Loss

The plot in fig.38 illustrates the dominance of the LOS path in terms of minimal path loss, which is expected due to absence of obstructions. Reflections introduce additional path loss compared to direct LOS paths but can still provide a viable signal path when LOS is obstructed. The diffraction loss values, while included for completeness, require further refinement and validation to ensure their accuracy and physical relevance.

The plot of received power versus elevation angle (fig.39) is directly influenced by the minimal path losses determined previously. In the range of 45 to 135 degrees, where LOS paths dominate, the received power is relatively higher, due to the LOS paths experiencing minimal attenuation compared to reflected and diffracted paths. At angles outside 45-135 degree range, reflections become the primary mode of signal propagation. Reflected paths introduce more path loss, therefore the received power in the corresponding regions is lower than the LOS range, but higher than the regions where diffraction dominates. For elevation angles where neither LOS nor reflections occur, the received power is based on the diffracted path losses.

The transitions between different modes of propagation create noticeable discontinuities in the received plot. The abrupt changes indicate the switch from one dominant

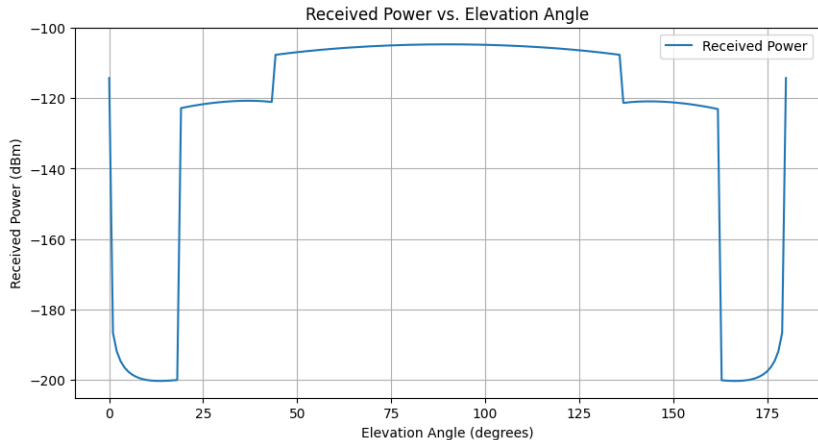


Figure 39: Received Power considering LOS, Reflected and Diffracted paths

propagation mode to another, each introducing different levels of attenuation.

The plot does show unexpected spikes in received power at lower elevation angles, which are anomalies due to the previously identified issues with the diffraction loss calculations leading to unrealistic path loss values. At low elevation angles, the expected received power should be minimal due to the greater path loss, as well as more pronounced ray bending. Therefore, the closer the satellite is to the horizon, the weaker the received signal should be due to the combined effects of longer path distance and high diffraction losses. To obtain physically accurate results, the diffraction model needs to be corrected.

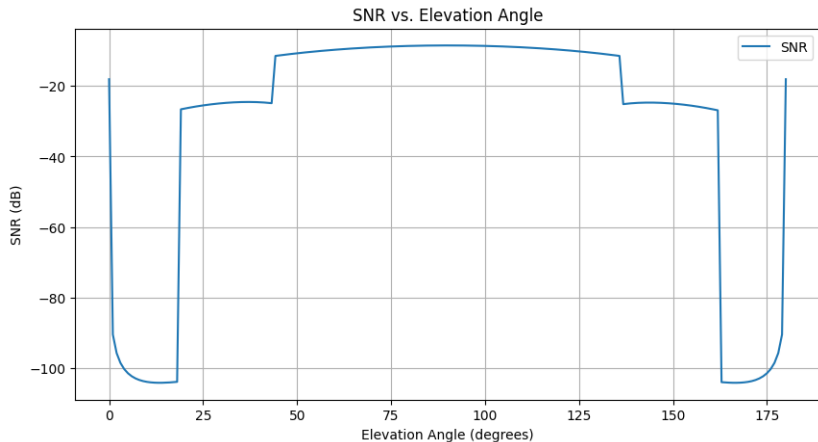


Figure 40: SNR considering LOS, Reflected and Diffracted paths

The Signal-to-Noise Ratio plot, illustrated in fig.40, follows a similar pattern to the received power plot, which is expected since SNR is directly influenced by the received signal strength. The SNR is highest between the elevation angles of approximately 45 degrees to 135 degrees, where the Line of Sight (LOS) path is available. This range corresponds to the minimal path loss, resulting in stronger received signals and, con-

sequently, higher SNR values. At elevation angles close to 0 and 180 degrees, the SNR drops significantly. This is due to the combination of increased path loss and erroneous diffraction losses. These angles correspond to situations where the signal path is obstructed, resulting in much higher path loss and lower received power.

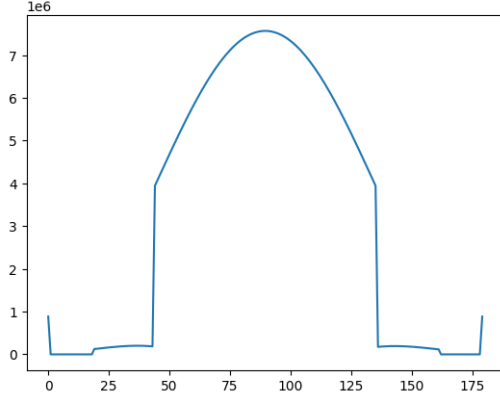


Figure 41: Channel capacity (bps) considering LOS, Reflected and Diffracted waves vs elevation angle

The channel capacity evaluation considers only the strongest multipath component at any given time, which means the plot seen in fig.41 primarily reflects the impact of the minimal path loss for each elevation angle. In the 45-135 degrees elevation angle range, the channel capacity is highest and coincides with the values obtained in Part 1, where LOS path loss was considered. The high capacity is due to the minimal path loss in this range, resulting in higher received power and SNR.

For low elevation angles, where LOS is obstructed, there is a significant decrease in channel capacity, associated with higher path losses of diffracted or reflected rays, leading to lower SNR. The unrealistic spikes and the sharp drop in channel capacity at very low elevation angles are artifacts resulting from the erroneous diffraction loss calculations mentioned earlier. These artifacts indicate that the channel capacity values in these regions are not physically meaningful.

4.5 Limitations and Further Work

Due to the identified issues with the diffraction loss model, the current channel capacity evaluation for non-LOS angles is not accurate. Further work is needed to refine the model and provide a more accurate assessment.

The total transmitted data, which would typically be determined by evaluating the area under the channel capacity curve, has not been calculated due to these inaccuracies.

Additionally, an analysis using antenna arrays instead of a single isotropic antenna as the receiver could not be completed due to time constraints.

By addressing these issues and refining the models, future evaluations can provide more reliable insights into the channel capacity and overall performance of the communication system.

5 Conclusion

In the initial part of the project, an analysis of the communication link in a free space environment has been performed, focusing on line-of-sight (LOS) communication between a satellite and a ground receiver. This involved:

- Evaluating the path loss over a range of elevation angles from 0 to 180 degrees. The results indicated a decreasing trend in path loss with increasing elevation angle, reaching a minimum at the zenith (90 degrees), consistent with theoretical expectations due to the shortest distance between the satellite and receiver.
- Calculating the received power using the path loss values. The received power was highest at mid-range elevation angles, correlating with lower path losses. The signal-to-noise ratio (SNR) assessment was based on the received power and system noise. The highest SNR values were observed when the satellite is positioned at zenith.
- Estimating the channel capacity, which showed maximum values at mid-range elevation angles where path loss and noise were minimal.
- Considering the impact of rain at different exceedances, which showed a significant reduction in received power and SNR, particularly at lower elevation angles.

The second part of the project extended the analysis by considering the ground station equipped with Uniform Linear Arrays (ULA) of isotropic and patch antennas:

- The gain patterns for different ULA configurations were computed, demonstrating enhanced directivity and increased gain with more elements in the array.
- The use of ULAs showed significant improvements in received power compared to a single isotropic antenna. Patch arrays, due to their directional nature, provided even higher gains at zenith angles.
- The SNR improved significantly with the use of antenna arrays. Positive SNR values were achieved over a broader range of elevation angles, enhancing the link quality.
- The channel capacity increased with the number of elements in the array. The total transmitted data during one satellite pass was significantly higher with ULAs, especially for patch antenna arrays.

The third part of the project introduced a more realistic scenario with two buildings adjacent to the ground station, incorporating multipath components (LOS, reflections, and diffraction):

- The LOS path loss was confirmed for elevation angles between 45 to 135 degrees where no obstructions occurred.
- Reflections were considered for elevation angles where LOS was obstructed. The reflected path loss showed additional attenuation compared to LOS paths.

- Diffraction was evaluated using the knife-edge model. However, the results were found to be inconsistent with physical expectations, suggesting an error in the implementation. This was identified as a limitation needing further investigation.
- The received power, SNR, and channel capacity were re-evaluated considering the strongest multipath component at each elevation angle, highlighting the limitations of NLOS communication.
- The current diffraction model's inaccuracies affected the overall evaluation, particularly at low elevation angles. Further work is required to refine this model and accurately assess the impact of diffracted paths. Additionally, the implementation of antenna arrays in this complex scenario was not completed due to time constraints, representing an area for future research.

This comprehensive analysis provided valuable insights into the performance of LEO satellite communication links under different scenarios. The findings highlight the importance of considering multiple propagation paths and advanced antenna configurations to optimize link performance. Future work should focus on refining the diffraction model and completing the analysis with antenna arrays to provide a more holistic understanding of satellite-ground station communication in realistic environments.

References

- [1] Recommendation ITU-R P.618-14 (08/2023): Propagation data and prediction methods required for the design of Earth-space telecommunication systems
- [2] Recommendation ITU-R P.837-7 (06/2017): Characteristics of precipitation for propagation modelling